Computer Methods in Applied Mechanics and Engineering 458 (2026) 118790

Contents lists available at ScienceDirect

Comput. Methods Appl. Mech. Engrg.

journal homepage: www.elsevier.com/locate/cma

Port-Hamiltonian formulation and structure-preserving discretization of finite elasticity based on a mixed Hu-Washizu-type formulation

Moritz Hille *, Peter Betsch , Marlon Franke

Institute of Mechanics, Karlsruhe Institute of Technology (KIT), Germany

ARTICLE INFO

Keywords:
Nonlinear elastodynamics
Livens principle
Hu-Washizu principle
Port-Hamiltonian formulation
Mixed finite elements
Energy-momentum methods

ABSTRACT

We propose a port-Hamiltonian formulation and structure-preserving discretization of finite elasticity. The energy functional (or Hamiltonian) is based on a polyconvex representation of the stored energy and gives rise to three strain-type fields, which play the role of energy variables in the port-Hamiltonian formulation. We show that a Hu-Washizu-type extension of the variational principle of Livens can be used (i) to derive the continuous port-Hamiltonian formulation and (ii) to perform a structure-preserving spatial discretization. In particular, we show that the spatial finite element discretization of the underlying mixed formulation yields a discrete port-Hamiltonian system. Moreover, the temporal discretization of the underlying continuous formulation yields a new energy-momentum consistent framework, which accommodates alternative finite element formulations. The new framework, in particular, covers mixed finite elements that have been shown to be well suited for handling quasi-incompressible material behavior. Numerical examples are provided to evaluate the numerical performance and stability of the newly devised energy-momentum schemes.

1. Introduction

The port-Hamiltonian (pH) formulation of evolution equations related to multiphysics systems provides an appealing framework for modeling, simulation, and control [1,2]. The energy-based pH description takes into account dissipation and interaction with the environment by means of ports, and can thus be considered as an extension of classical Hamiltonian systems to open systems.

Finite-dimensional pH systems have been originally introduced in [3] and are based on a Dirac structure, which encodes system properties such as passivity and energy consistency into system equations. The extension of the pH modeling paradigm to infinite-dimensional systems is based on a Stokes-Dirac structure and can be traced back to [4]. Since then, distributed pH systems have been subject to extensive research in the areas of multiphysics system modeling, analysis and design of control techniques, and structure-preserving discretization methods, as categorized in the comprehensive literature review [5].

The design of structure-preserving discretization techniques is a natural objective in preserving the intrinsic structure and properties of pH systems, such as passivity and energy consistency. Galerkin-based numerical methods for the structure-preserving discretization of pH systems have become more popular only recently [6]. In particular, finite element methods have been applied to discretize pH formulations of viscoelastic strings [7], beams [8–11], plates [12], the wave equation [13], poroelasticity [14], and

* Corresponding author.
E-mail address: peter.betsch@kit.edu (P. Betsch).

https://doi.org/10.1016/j.cma.2026.118790
Received 30 September 2025; Received in revised form 1 January 2026; Accepted 27 January 2026
Available online 29 April 2026

thermoelasticity [15]. It is important to note that the typical use of energy variables in the pH approach inherently gives rise to mixed finite element formulations.

Interestingly, the field of nonlinear elastodynamics has been addressed only very recently within the pH framework. The pH structure of the so-called velocity-stress formulation proposed in [16] led to the design of a linear implicit energy-consistent time-stepping scheme. Similarly, the linearly implicit energy-momentum (EM) scheme developed in [17] is based on a mixed finite element description relying on the approximation of the displacement, velocity and stress fields. Both works [16,17] are closely related to the Hellinger-Reissner variational formulation and restricted to the St. Venant-Kirchhoff material. The pH formulation proposed in [18] is based on the approximation of displacement, linear momentum density, and Green-Lagrangian strain fields and takes into account general hyperelastic constitutive laws. While the semi-discrete equations of motion in [18] retain the pH structure, the Störmer-Verlet scheme or the midpoint rule are used in the temporal discretization, thus generally compromising the balance law for energy in the discrete model.

The above summarized developments in the framework of the pH formulation complement earlier works on the design of EM schemes for nonlinear elastodynamics. In fact, the quest for numerically stable time-stepping schemes led to the first EM scheme for non-linear elastodynamics proposed in the pioneering work [19]. This method has been developed in the framework of purely displacement-based finite elements and relies on a modification of the implicit midpoint rule on the constitutive level. This modification was then generalized for arbitrary hyperelastic materials applying the notion of discrete derivative in [20]. In essence, the application of discrete derivatives at the constitutive level yields specific stress formulas that are a prominent feature of EM methods [21]. It should be noted that EM schemes can also be designed by applying Galerkin methods in time [22]. In particular, higher-order EM schemes have been devised in [23]. EM schemes have also been developed in the framework of mixed finite elements resulting from a polyconvex representation of hyperelastic materials [24].

In the present work, we propose a new pH-based avenue for the design of EM schemes for finite-deformation elastodynamics. Similarly to [24], we start from a polyconvex representation of hyperelastic materials. The proposed pH-based approach makes it possible to accommodate alternative mixed finite element formulations, leading to related EM methods. In this way, previously developed mixed finite elements which have been shown to perform well in finite-deformation problems, including quasi-imcompressible material behavior, can be extended to the dynamic regime. This will be shown by incorporating the family of mixed finite elements developed in [25,26] into the present approach.

The outline of the rest of the paper is as follows. Section 2 provides a mixed variational principle for finite strain elastodynamics, from which the continuous pH formulation will be derived. The corresponding weak form of the fully mixed formulation provides the starting point for the energy-momentum consistent temporal discretization, as discussed in Section 3. Section 4 shows that the spatial discretization of the fully mixed weak form yields semidiscrete equations of motion which fit into the framework of discrete pH systems. Starting from the time-discrete weak form of the underlying fully mixed description, alternative spatial discretizations are incorporated in Section 5, leading to corresponding EM schemes. Numerical investigations are presented in Section 6 and conclusions are drawn in Section 7.

2. Port-Hamiltonian formulation of nonlinear elastodynamics

This section introduces the theoretical framework underlying the proposed pH formulation of nonlinear elastodynamics. We begin by reviewing the fundamentals of continuum mechanics and the tensor cross product. A polyconvex energy density function is introduced afterwards, and a variational principle is used to derive the strong form of the governing equations. The local field equations are reformulated in port-Hamiltonian form, and alternative reduced-order pH formulations are briefly discussed. We proceed with the derivation of the weak form and conclude by verifying the balance laws for energy and angular momentum.

2.1. Quantities of continuum mechanics and tensor cross product

We consider a deformable body in the reference configuration $\Omega_0 \subset \mathbb{R}^3$, depicted in Fig. 1, which can be described by material points $\mathbf{X} \in \mathbb{R}^3$. The mapping $\mathbf{x}(t) = \boldsymbol{\varphi}(\mathbf{X}, t)$ maps points $\mathbf{X}$ to their corresponding points $\mathbf{x} = \mathbf{x}(t) \in \mathbb{R}^3$ of the body in the spatial configuration Ω at time t, i.e. $\Omega(t) = \boldsymbol{\varphi}(\Omega_0, t) \subset \mathbb{R}^3$ for a time $t \in \mathcal{I} = [t_0, t_N]$, where $\mathcal{I}$ is the time interval of interest. The boundary of the domain $\partial\Omega_0$ is disjointly decomposed into the Dirichlet boundary $\partial_\varphi\Omega_0$ with prescribed placements $\bar{\boldsymbol{\varphi}}(t)$, and the Neumann boundary $\partial_\sigma\Omega_0$ with prescribed tractions $\bar{\mathbf{t}} = \bar{\mathbf{t}}(t)$. In addition, there are prescribed body forces $\bar{\mathbf{g}} = \bar{\mathbf{g}}(t) \in \mathbb{R}^3$ and distributed body control forces $\bar{\mathbf{b}} = \bar{\mathbf{b}}(t) \in \mathbb{R}^3$ acting on the body.

To map material line elements $\mathrm{d}\mathbf{X}$ to their spatial counterparts $\mathrm{d}\mathbf{x}$, we introduce the deformation gradient $\mathbf{F}_\varphi$, a second-order tensor given by

$$\mathrm{d}\mathbf{x} = \mathbf{F}_\varphi \mathrm{d}\mathbf{X} \,, \quad \mathbf{F}_\varphi = \nabla\boldsymbol{\varphi}(\mathbf{X}, t) \,, \tag{1}$$

where ∇ denotes the gradient with respect to the material coordinates. Note that the notation $\mathbf{F}_\varphi$ explicitly indicates that the deformation gradient depends on the deformation map. This notation is used in the sequel to distinguish deformation-dependent quantities from associated quantities of the mixed formulation.

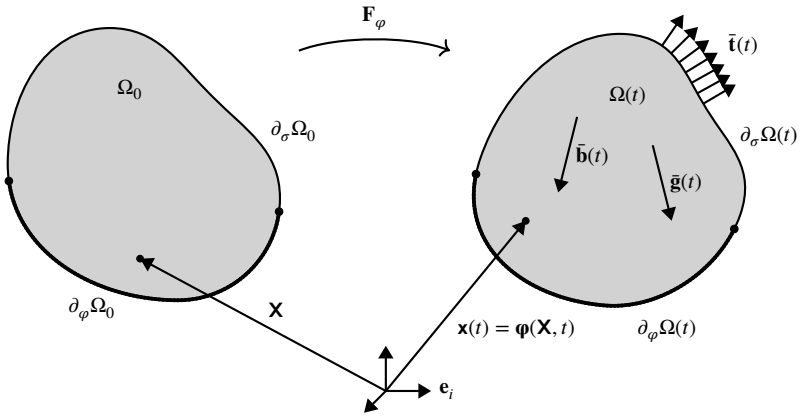

Fig. 1. Configuration and kinematics of a deformable body Ω

In this paper, we use the so-called tensor cross product[1] between two second-order tensors $\mathbf{A}, \mathbf{B} \in \mathbb{R}^{3\times3}$ given by

$$(\mathbf{A} \gg\!\ll \mathbf{B})_{ij} = \epsilon_{i\alpha\beta}\epsilon_{jab}A_{\alpha a}B_{\beta b} \,, \tag{2}$$

where repeated indices $a, b, \alpha, \beta, i, j \in \{1, 2, 3\}$ imply summation according to Einstein's convention and ϵ_{ijk} denotes the third-order permutation tensor. The tensor cross product can be used to rewrite the cofactor and the determinant of a second-order tensor $\mathbf{A}$ as

$$\begin{aligned} \operatorname{cof}(\mathbf{A}) &= \frac{1}{2}\,\mathbf{A} \gg\!\ll \mathbf{A} \,, \\ \det(\mathbf{A}) &= \frac{1}{6}(\mathbf{A} \gg\!\ll \mathbf{A}) : \mathbf{A} \,. \end{aligned} \tag{3}$$

This reformulation allows for some straightforward calculations due to suitable properties of the tensor cross product, given by

$$\begin{aligned} &\mathbf{A} \gg\!\ll \mathbf{B} = \mathbf{B} \gg\!\ll \mathbf{A} \\ &\mathbf{A} \gg\!\ll (\mathbf{B} + \mathbf{C}) = \mathbf{A} \gg\!\ll \mathbf{B} + \mathbf{A} \gg\!\ll \mathbf{C} \\ &(\mathbf{A} \gg\!\ll \mathbf{B}) : \mathbf{C} = (\mathbf{A} \gg\!\ll \mathbf{C}) : \mathbf{B} = (\mathbf{B} \gg\!\ll \mathbf{C}) : \mathbf{A} \,. \end{aligned} \tag{4}$$

In addition to the deformation gradient $\mathbf{F}_\varphi$, further kinematic measures can be introduced. These include the right Cauchy-Green deformation tensor, defined as

$$\mathbf{C}_\varphi = \mathbf{F}_\varphi^{\mathrm{T}}\mathbf{F}_\varphi \,, \tag{5}$$

as well as its cofactor,

$$\mathbf{G}_\varphi = \operatorname{cof}(\mathbf{C}_\varphi) = \frac{1}{2}\,\mathbf{C}_\varphi \gg\!\ll \mathbf{C}_\varphi \,, \tag{6}$$

and the determinant of the deformation gradient,

$$J_\varphi = \det(\mathbf{F}_\varphi) = \frac{1}{6}\left(\mathbf{F}_\varphi \gg\!\ll \mathbf{F}_\varphi\right) : \mathbf{F}_\varphi = \sqrt{\det(\mathbf{C}_\varphi)} \,. \tag{7}$$

The latter two expressions have been reformulated in terms of the tensor cross product to facilitate its efficient numerical implementation.

2.2. Polyconvex energy density function and equations of motion

Polyconvexity is a widely accepted notion for hyperelastic materials in the large-deformation regime. Consequently, we assume that the material behavior under consideration can be described by a polyconvex energy density function

$$W = \widehat{W}(\mathbf{F}_\varphi) = \widetilde{\mathcal{W}}\big(\mathbf{F}_\varphi, \operatorname{cof}(\mathbf{F}_\varphi), \det(\mathbf{F}_\varphi)\big) \,, \tag{8}$$

where $\widetilde{\mathcal{W}}$ is constructed to be convex with respect to its arguments. To obtain an objective representation, W is re-expressed as

$$W = \widehat{\mathcal{W}}(\mathbf{C}_\varphi) = \widetilde{\mathcal{W}}\big(\mathbf{C}_\varphi, \mathbf{G}_\varphi, J_\varphi\big) \tag{9}$$

with the kinematic measures $\mathbf{C}_\varphi$, $\mathbf{G}_\varphi$ and J_φ defined in (6) and (7).

[1] The tensor cross product can be found in [27] and its advantageous use has been more recently advocated in [28].

To derive the governing equations for the motion of an elastic body, we employ a Hu-Washizu-type extension of Livens' principle based on the variational functional, defined as

$$\begin{aligned} S = \int_{t_0}^{t_N} \int_{\Omega_0} \Big[\frac{1}{2}\rho_0 \mathbf{v}\cdot\mathbf{v} - \widetilde{\mathcal{W}}(\mathbf{C},\mathbf{G},J) + \boldsymbol{\pi}\cdot(\dot{\boldsymbol{\varphi}}-\mathbf{v}) - \boldsymbol{\Lambda}_{\mathbf{C}} : \big(\mathbf{C}_\varphi - \mathbf{C}\big) - \boldsymbol{\Lambda}_{\mathbf{G}} : \big(\mathbf{G}_\varphi - \mathbf{G}\big) - \lambda\big(J_\varphi - J\big) \Big] \mathrm{dV}\,\mathrm{dt} \\ + \int_{t_0}^{t_N} \left[\int_{\Omega_0} (\bar{\mathbf{g}} + \bar{\mathbf{b}})\cdot\boldsymbol{\varphi}\,\mathrm{dV} + \int_{\partial_\sigma\Omega_0} \bar{\mathbf{t}}\cdot\boldsymbol{\varphi}\,\mathrm{dA} \right] \mathrm{dt}\,, \end{aligned} \tag{10}$$

where $\rho_0 = \rho_0(\mathbf{X})$ is the mass density in reference configuration. Here, the displacement field $\boldsymbol{\varphi} \in \mathcal{V}_\varphi$ is sought in the function space

$$\mathcal{V}_\varphi = \big\{ \boldsymbol{\varphi} : \Omega_0 \to \mathbb{R}^3 \,|\, \varphi_i \in H^1(\Omega_0) \wedge \boldsymbol{\varphi} = \bar{\boldsymbol{\varphi}} \text{ on } \partial_\varphi\Omega_0 \big\}\,, \tag{11}$$

where $H^1(\Omega_0)$ is the Sobolev space. Similarly, the velocity field $\mathbf{v} \in \mathcal{V}_v$, where the function space $\mathcal{V}_v$ is defined as

$$\mathcal{V}_v = \big\{ \mathbf{v} : \Omega_0 \to \mathbb{R}^3 \,|\, v_i \in L^2(\Omega_0) \big\}\,, \tag{12}$$

where $L^2(\Omega_0)$ is the space of square-integrable functions on Ω_0. The kinematic variables $\mathbf{C} \in \mathcal{V}_C$, $\mathbf{G} \in \mathcal{V}_G$ and $J \in \mathcal{V}_J$ are introduced as independent fields representing the right Cauchy-Green tensor, its cofactor, and the determinant of the deformation gradient, respectively. Their equivalence with deformation-dependent measures $\mathbf{C}_\varphi$, $\mathbf{G}_\varphi$, and J_φ is enforced via the tensor-valued Lagrange multipliers $\boldsymbol{\Lambda}_{\mathbf{C}} \in \mathcal{V}_C$, $\boldsymbol{\Lambda}_{\mathbf{G}} \in \mathcal{V}_G$ and the scalar-valued Lagrange multiplier $\lambda \in \mathcal{V}_J$. The function spaces of the mixed variables and their Lagrange multipliers are defined as

$$\begin{aligned} \mathcal{V}_C = \mathcal{V}_G &= \big\{ \mathbf{A} : \Omega_0 \to \mathbb{S} \,|\, A_{ij} \in L^2(\Omega_0) \big\}\,, \\ \mathcal{V}_J &= \big\{ J : \Omega_0 \to \mathbb{R}_+ \backslash \{0\} \,|\, J \in L^2(\Omega_0) \big\}\,, \end{aligned} \tag{13}$$

where $\mathbb{S}$ is the space of symmetric 3×3 matrices. Note that in the functional S, the velocity field $\mathbf{v} \in \mathcal{V}_v$ is introduced as an independent field that is linked to the time derivative of the deformation field $\dot{\boldsymbol{\varphi}}$ through the vector-valued Lagrange multiplier $\boldsymbol{\pi} \in \mathcal{V}_v$.

Imposing the stationarity of the functional S yields the associated Euler-Lagrange equations. Accordingly, we obtain $\boldsymbol{\pi} = \rho_0\mathbf{v}$, such that the multiplier $\boldsymbol{\pi}$ corresponds to the linear momentum density. In addition to that, the remaining stationary conditions read

$$\left.\begin{aligned} \dot{\boldsymbol{\varphi}} &= \mathbf{v} \\ \rho_0\,\dot{\mathbf{v}} &= \mathrm{Div}(\mathbf{F}_\varphi\mathbf{S}) + \bar{\mathbf{g}} + \bar{\mathbf{b}} \\ \boldsymbol{\Lambda}_{\mathbf{C}} &= \partial_{\mathbf{C}}\widetilde{\mathcal{W}}(\mathbf{C},\mathbf{G},J) \\ \boldsymbol{\Lambda}_{\mathbf{G}} &= \partial_{\mathbf{G}}\widetilde{\mathcal{W}}(\mathbf{C},\mathbf{G},J) \\ \lambda &= \partial_J\widetilde{\mathcal{W}}(\mathbf{C},\mathbf{G},J) \\ \mathbf{C} &= \mathbf{C}_\varphi \\ \mathbf{G} &= \mathbf{G}_\varphi \\ J &= J_\varphi \end{aligned}\right\} \text{in } \Omega_0\times\mathcal{I}\,, \tag{14}$$

where the second Piola-Kirchhoff stress tensor is given by

$$\mathbf{S} = 2\boldsymbol{\Lambda}_{\mathbf{C}} + 2\boldsymbol{\Lambda}_{\mathbf{G}} \Subset \mathbf{C}_\varphi + \frac{\lambda}{J_\varphi}\mathbf{G}_\varphi\,. \tag{15}$$

Note that in (14), the velocity field has been preferred over the linear momentum density field, since in the discretization process we prefer to use the velocity field.

In addition to the local field equations (14), the stationarity of functional S implies the boundary condition

$$\mathbf{F}_\varphi\mathbf{S}\mathbf{N} = \bar{\mathbf{t}} \text{ on } \partial_\sigma\Omega_0\,, \tag{16}$$

where $\mathbf{N}$ denotes the unit outward normal vector on the boundary $\partial_\sigma\Omega_0$. Note that during the imposition of the stationarity of functional S, the usual end point conditions on the deformation field at times t_0 and t_N have been taken into account for all $\mathbf{X} \in \Omega_0$.

Remark 1. Functional S in (10) can be viewed as a combination of Livens' variational principle (see [29]) and the Hu-Washizu principle (see the 'generalized principle' in [30]) adapted to polyconvex elasticity. In addition to the Lagrange multipliers $\boldsymbol{\pi}$ and $\{\boldsymbol{\Lambda}_{\mathbf{C}}, \boldsymbol{\Lambda}_{\mathbf{G}}, \lambda\}$, another vector-valued Lagrange multiplier could be used to enforce Dirichlet boundary conditions $\boldsymbol{\varphi} = \bar{\boldsymbol{\varphi}}$ on $\partial_\varphi\Omega_0$ (cf. [30]). This contrasts to our present approach, in which the Dirichlet boundary conditions are taken into account by choosing $\boldsymbol{\varphi} \in \mathcal{V}_\varphi$.

2.3. Port-Hamiltonian form of the local field equations

Next, we bring the local field equations into port-Hamiltonian form. To identify the energy variables relevant for the port-Hamiltonian formulation, we introduce the total energy of the elastic body, also called the *Hamiltonian* functional. Accordingly, we define

$$\mathcal{H}(\mathbf{x}) = \int_{\Omega_0} \big(\frac{1}{2}\rho_0\mathbf{v}\cdot\mathbf{v} + \widetilde{\mathcal{W}}(\mathbf{C},\mathbf{G},J) - \bar{\mathbf{g}}\cdot\boldsymbol{\varphi} \big)\,\mathrm{dV}\,. \tag{17}$$

Note that the potential of body forces $\bar{\mathbf{g}}$ has been included in the Hamiltonian, while external tractions $\bar{\mathbf{t}}$ acting on the boundary of the elastic body, as well as distributed control body forces $\bar{\mathbf{b}}$ are treated as inputs in the port-Hamiltonian formulation. The specific form of (17) gives rise to the energy variables

$$\mathbf{x} = \begin{bmatrix} \boldsymbol{\varphi} \\ \mathbf{v} \\ \mathbf{C} \\ \mathbf{G} \\ J \end{bmatrix}. \tag{18}$$

Now, the functional derivative of the Hamiltonian can be written as

$$\delta_{\mathbf{x}}\mathcal{H}(\mathbf{x}) = \begin{bmatrix} -\bar{\mathbf{g}} \\ \rho_0 \mathbf{v} \\ \partial_{\mathbf{C}}\widetilde{\mathcal{W}} \\ \partial_{\mathbf{G}}\widetilde{\mathcal{W}} \\ \partial_J \widetilde{\mathcal{W}} \end{bmatrix}. \tag{19}$$

The goal is now to bring the local field equations of the present problem into pH form, which is given by

$$\begin{aligned} \mathcal{E}\dot{\mathbf{x}} &= \mathcal{J}(\mathbf{x})\mathbf{z}(\mathbf{x}) + \mathcal{B}\mathbf{u}\,, \\ \mathbf{y} &= \mathcal{B}^*\mathbf{z}(\mathbf{x})\,, \end{aligned} \tag{20}$$

where

$$\mathcal{E}^{\mathrm{T}}\mathbf{z}(\mathbf{x}) = \delta_{\mathbf{x}}\mathcal{H}(\mathbf{x}) \tag{21}$$

(see [31,32]). In particular, we need to identify the differential operator $\mathcal{J}(\mathbf{x})$ along with matrix $\mathcal{E}$ from the local field equations. Note that $\mathcal{B}$ is a differential operator that can account for distributed controls $\mathbf{u}$ acting on the system. The collocated and power-conjugated outputs $\mathbf{y}$ are defined in the second equation of (20), where $\mathcal{B}^*$ denotes the adjoint of $\mathcal{B}$. The vector-valued function $\mathbf{z}(\mathbf{x})$ is defined in equation (21) in terms of the variational derivative of the Hamiltonian. We first rewrite the local field equations (14) as

$$\left.\begin{aligned} \dot{\boldsymbol{\varphi}} &= \mathbf{v} \\ \rho_0\,\dot{\mathbf{v}} &= \mathrm{Div}(\mathbf{F}_\varphi \mathbf{S}) + \bar{\mathbf{g}} + \bar{\mathbf{b}} \\ \boldsymbol{\Lambda}_{\mathbf{C}} &= \partial_{\mathbf{C}}\widetilde{\mathcal{W}}(\mathbf{C},\mathbf{G},J) \\ \boldsymbol{\Lambda}_{\mathbf{G}} &= \partial_{\mathbf{G}}\widetilde{\mathcal{W}}(\mathbf{C},\mathbf{G},J) \\ \lambda &= \partial_J \widetilde{\mathcal{W}}(\mathbf{C},\mathbf{G},J) \\ \dot{\mathbf{C}} &= \tfrac{\mathrm{d}}{\mathrm{d}t}\mathbf{C}_\varphi = 2\,\mathrm{sym}(\mathbf{F}_\varphi^{\mathrm{T}}\nabla\mathbf{v}) \\ \dot{\mathbf{G}} &= \tfrac{\mathrm{d}}{\mathrm{d}t}\mathbf{G}_\varphi = 2\mathbf{C}_\varphi \mathbin{⋘} \mathrm{sym}(\mathbf{F}_\varphi^{\mathrm{T}}\nabla\mathbf{v}) \\ \dot{J} &= \tfrac{\mathrm{d}}{\mathrm{d}t}J_\varphi = J_\varphi^{-1}\mathbf{G}_\varphi : \mathrm{sym}(\mathbf{F}_\varphi^{\mathrm{T}}\nabla\mathbf{v}) \end{aligned}\right\} \text{in } \Omega_0 \times \mathcal{I}\,, \tag{22}$$

Note that the second Piola-Kirchhoff stress tensor $\mathbf{S}$ has been defined in (15) and thus follows from the constitutive relations for the Lagrange multipliers $\{\boldsymbol{\Lambda}_{\mathbf{C}}, \boldsymbol{\Lambda}_{\mathbf{G}}, \lambda\}$ in (22). The last three equations in (22) comprise the kinematic relationships in rate form, as required by the pH form (20). It is now straightforward to put (22) in pH form (20) by substituting the expressions for the Lagrange multipliers from (22) into (15). Consequently, we arrive at the differential operator $\mathcal{J}(\mathbf{x})$ given by the expression

$$\mathcal{J}(\mathbf{x}) = \begin{bmatrix} 0 & I & 0 & 0 & 0 \\ -I & 0 & \mathrm{Div}(2\mathbf{F}_\varphi \square) & \mathrm{Div}(2\mathbf{F}_\varphi \mathbf{C}_\varphi \mathbin{⋘} \square) & \mathrm{Div}(J_\varphi^{-1}\mathbf{F}_\varphi \mathbf{G}_\varphi \square) \\ 0 & 2\,\mathrm{sym}(\mathbf{F}_\varphi^{\mathrm{T}}\nabla(\square)) & 0 & 0 & 0 \\ 0 & 2\mathbf{C}_\varphi \mathbin{⋘} \mathrm{sym}(\mathbf{F}_\varphi^{\mathrm{T}}\nabla(\square)) & 0 & 0 & 0 \\ 0 & J_\varphi^{-1}\mathbf{G}_\varphi : \mathrm{sym}(\mathbf{F}_\varphi^{\mathrm{T}}\nabla(\square)) & 0 & 0 & 0 \end{bmatrix}, \tag{23}$$

together with matrices $\mathcal{E}$ and $\mathcal{B}$, which assume the form

$$\mathcal{E} = \mathcal{E}^{\mathrm{T}} = \begin{bmatrix} I & 0 & 0 & 0 & 0 \\ 0 & \rho_0 I & 0 & 0 & 0 \\ 0 & 0 & I & 0 & 0 \\ 0 & 0 & 0 & I & 0 \\ 0 & 0 & 0 & 0 & I \end{bmatrix} \quad \text{and} \quad \mathcal{B} = \begin{bmatrix} 0 & 0 & 0 & 0 & 0 \\ 0 & I & 0 & 0 & 0 \\ 0 & 0 & 0 & 0 & 0 \\ 0 & 0 & 0 & 0 & 0 \\ 0 & 0 & 0 & 0 & 0 \end{bmatrix}. \tag{24}$$

In (23) and (24), I denotes the identity operator. The vector of distributed controls $\mathbf{u}$ in (20) contains the distributed control body forces $\bar{\mathbf{b}}$.

Note that the differential operator $\mathcal{J}(\mathbf{x})$ is formally skew-adjoint, i.e., $\mathcal{J}(\mathbf{x}) = -\mathcal{J}(\mathbf{x})^*$. This property is reflected in the power balance as can be seen below. Taking the time derivative of the Hamiltonian yields

$$\dot{\mathcal{H}}(\mathbf{x}) = \langle \delta_{\mathbf{x}}\mathcal{H}(\mathbf{x}), \dot{\mathbf{x}} \rangle\,, \tag{25}$$

where the brackets represent the duality pairing. Using (20), we obtain

$$\begin{aligned}\dot{\mathcal{H}}(\mathbf{x}) &= \left\langle \mathcal{E}^{\mathrm{T}}\mathbf{z}(\mathbf{x}), \dot{\mathbf{x}} \right\rangle \\ &= \langle \mathbf{z}(\mathbf{x}), \mathcal{E}\dot{\mathbf{x}} \rangle \\ &= \langle \mathbf{z}(\mathbf{x}), \mathcal{J}(\mathbf{x})\mathbf{z}(\mathbf{x}) \rangle + \langle \mathbf{z}(\mathbf{x}), \mathcal{B}\mathbf{u} \rangle \, .\end{aligned} \tag{26}$$

Now, after a straightforward calculation, the first term on the right-hand side of the last equation yields

$$\begin{aligned}\langle \mathbf{z}(\mathbf{x}), \mathcal{J}(\mathbf{x})\mathbf{z}(\mathbf{x}) \rangle &= \left\langle \mathbf{v}, \mathrm{Div}(\mathbf{F}_\varphi \mathbf{S}) \right\rangle + \left\langle \nabla \mathbf{v}, \mathbf{F}_\varphi \mathbf{S} \right\rangle \\ &= \int_{\partial_\sigma \Omega_0} \bar{\mathbf{t}} \cdot \mathbf{v} \, \mathrm{dA} \, ,\end{aligned} \tag{27}$$

where Green's theorem along with the Neumann boundary condition have been used. Furthermore, the second term on the right-hand side of (26) leads to

$$\langle \mathbf{z}(\mathbf{x}), \mathcal{B}\mathbf{u} \rangle = \langle \mathcal{B}^* \mathbf{z}(\mathbf{x}), \mathbf{u} \rangle = \langle \mathbf{y}, \mathbf{u} \rangle \, . \tag{28}$$

Thus, the resulting power balance takes the form

$$\dot{\mathcal{H}}(\mathbf{x}) = \int_{\partial_\sigma \Omega_0} \bar{\mathbf{t}} \cdot \mathbf{v} \, \mathrm{dA} + \langle \mathbf{y}, \mathbf{u} \rangle \, . \tag{29}$$

Note that the contribution to the power balance of the potential body forces $\bar{\mathbf{g}}$ emanates from the Hamiltonian on the left-hand side of the last equation.

2.4. Weak form

In the following, we introduce the weak form associated with the pH formulation of the local field equations dealt with in Section 2.3. We therefore start with the set of equations given in (22). Multiplying these equations by admissible test functions $\{\mathbf{w}_\pi, \mathbf{w}_\varphi\}$, $\left\{\mathbf{w}_{\mathbf{\Lambda}_\mathbf{C}}, \mathbf{w}_{\mathbf{\Lambda}_\mathbf{G}}, w_\lambda\right\}$ and $\{\mathbf{w}_\mathbf{C}, \mathbf{w}_\mathbf{G}, w_J\}$, subsequently integrating over body Ω_0 and performing an integration by parts yields the weak form

$$\begin{aligned}
&\int_{\Omega_0} \mathbf{w}_\pi \cdot (\dot{\boldsymbol{\varphi}} - \mathbf{v}) \, \mathrm{dV} = 0 \\
&\int_{\Omega_0} \mathbf{w}_\varphi \cdot \rho_0 \dot{\mathbf{v}} + 2\,\mathrm{sym}(\mathbf{F}_\varphi^{\mathrm{T}} \nabla \mathbf{w}_\varphi) : \left(\mathbf{\Lambda}_\mathbf{C} + \mathbf{\Lambda}_\mathbf{G} \lll \mathbf{C}_\varphi + \frac{\lambda}{2J_\varphi}\mathbf{G}_\varphi\right) \mathrm{dV} = \int_{\Omega_0} \mathbf{w}_\varphi \cdot (\bar{\mathbf{g}} + \bar{\mathbf{b}}) \, \mathrm{dV} + \int_{\partial\Omega_0} \mathbf{w}_\varphi \cdot \bar{\mathbf{t}} \, \mathrm{dA} \\
&\int_{\Omega_0} \mathbf{w}_\mathbf{C} : \left[\mathbf{\Lambda}_\mathbf{C} - \partial_\mathbf{C} \widetilde{\mathcal{W}}(\mathbf{C}, \mathbf{G}, J)\right] \mathrm{dV} = 0 \\
&\int_{\Omega_0} \mathbf{w}_\mathbf{G} : \left[\mathbf{\Lambda}_\mathbf{G} - \partial_\mathbf{G} \widetilde{\mathcal{W}}(\mathbf{C}, \mathbf{G}, J)\right] \mathrm{dV} = 0 \\
&\int_{\Omega_0} w_J \left[\lambda - \partial_J \widetilde{\mathcal{W}}(\mathbf{C}, \mathbf{G}, J)\right] \mathrm{dV} = 0 \\
&\int_{\Omega_0} \mathbf{w}_{\mathbf{\Lambda}_\mathbf{C}} : \left[\dot{\mathbf{C}} - 2\,\mathrm{sym}(\mathbf{F}_\varphi^{\mathrm{T}} \nabla \mathbf{v})\right] \mathrm{dV} = 0 \\
&\int_{\Omega_0} \mathbf{w}_{\mathbf{\Lambda}_\mathbf{G}} : \left[\dot{\mathbf{G}} - 2\mathbf{C}_\varphi \lll \mathrm{sym}(\mathbf{F}_\varphi^{\mathrm{T}} \nabla \mathbf{v})\right] \mathrm{dV} = 0 \\
&\int_{\Omega_0} w_\lambda \left[\dot{J} - J_\varphi^{-1} \mathbf{G}_\varphi : \mathrm{sym}(\mathbf{F}_\varphi^{\mathrm{T}} \nabla \mathbf{v})\right] \mathrm{dV} = 0 \, .
\end{aligned} \tag{W}$$

These equations hold for arbitrary $\mathbf{w}_\varphi \in \mathcal{V}_\varphi^0$ with

$$\mathcal{V}_\varphi^0 = \left\{ \mathbf{w}_\varphi : \Omega_0 \to \mathbb{R}^3 \mid w_{\varphi_i} \in H^1(\Omega_0) \wedge \mathbf{w}_\varphi = \mathbf{0} \text{ on } \partial_\varphi \Omega_0 \right\} \tag{30}$$

as well as arbitrary $\mathbf{w}_\pi \in \mathcal{V}_v$, $\mathbf{w}_\mathbf{C}, \mathbf{w}_\mathbf{G}, \mathbf{w}_{\mathbf{\Lambda}_\mathbf{C}}, \mathbf{w}_{\mathbf{\Lambda}_\mathbf{G}} \in \mathcal{V}_C$, and $w_J, w_\lambda \in \mathcal{V}_J$.

Note that we retain the constitutive equations for the Lagrange multipliers resulting from the underlying variational principle in weak form (W). As will be shown in the sequel, this facilitates an energy-momentum consistent spatial discretization in general (see also Remark 4).

2.5. Conservation properties

In the next step, conservation properties of the newly developed formulation are discussed. In particular, this is conservation of total energy and total angular momentum.

2.5.1. Conservation of total energy

Energy conservation in the time-continuous case is ensured if the time derivative of the Hamiltonian $\mathcal{H}$, defined in (17), vanishes, i.e.,

$$\dot{\mathcal{H}} = \frac{\mathrm{d}}{\mathrm{dt}} \left[\int_{\Omega_0} \left(\frac{1}{2} \rho_0 \mathbf{v} \cdot \mathbf{v} + \widetilde{\mathcal{W}}(\mathbf{C}, \mathbf{G}, J) - \bar{\mathbf{g}} \cdot \boldsymbol{\varphi} \right) \mathrm{dV} \right] = 0 \,. \tag{31}$$

To verify this, we choose the test functions $\mathbf{w}_\pi = -\rho_0 \dot{\mathbf{v}}$, $\mathbf{w}_\varphi = \dot{\boldsymbol{\varphi}}$, $\mathbf{w}_\mathbf{C} = -\dot{\mathbf{C}}$, $\mathbf{w}_\mathbf{G} = -\dot{\mathbf{G}}$, $w_J = -\dot{J}$, $\mathbf{w}_{\boldsymbol{\Lambda}_\mathbf{C}} = \boldsymbol{\Lambda}_\mathbf{C}$, $\mathbf{w}_{\boldsymbol{\Lambda}_\mathbf{G}} = \boldsymbol{\Lambda}_\mathbf{G}$, and $w_\lambda = \lambda$, and insert them into (W). Summing the resulting equations yields

$$\begin{aligned} &\int_{\Omega_0} \rho_0 \dot{\mathbf{v}} \cdot \mathbf{v} + \partial_\mathbf{C} \widetilde{\mathcal{W}} : \dot{\mathbf{C}} + \partial_\mathbf{G} \widetilde{\mathcal{W}} : \dot{\mathbf{G}} + \partial_J \widetilde{\mathcal{W}} \dot{J} - \dot{\boldsymbol{\varphi}} \cdot \bar{\mathbf{g}} \, \mathrm{dV} \\ &\quad = \int_{\partial_\sigma \Omega_0} \dot{\boldsymbol{\varphi}} \cdot \bar{\mathbf{t}} \, \mathrm{dA} + \int_{\Omega_0} \dot{\boldsymbol{\varphi}} \cdot \bar{\mathbf{b}} \, \mathrm{dV} \,, \end{aligned} \tag{32}$$

which coincides with (31) precisely in the absence of boundary tractions and distributed control body forces, that is, $\bar{\mathbf{t}} = \mathbf{0}$ and $\bar{\mathbf{b}} = \mathbf{0}$. It should be noted that the kinematic relation $\dot{\boldsymbol{\varphi}} = \mathbf{v}$ is used to obtain (32).

2.5.2. Conservation of angular momentum

The angular momentum of the body Ω_0 is defined as

$$\mathbf{L} = \int_{\Omega_0} \boldsymbol{\varphi} \times \mathbf{v} \rho_0 \, \mathrm{dV} \,. \tag{33}$$

It is conserved if the time derivative of $\mathbf{L}$ vanishes, i.e.,

$$\dot{\mathbf{L}} = \int_{\Omega_0} \frac{\mathrm{d}}{\mathrm{dt}} \left(\boldsymbol{\varphi} \times \mathbf{v} \rho_0 \right) \mathrm{dV} = \mathbf{0} \,. \tag{34}$$

In analogy to the energy conservation proof, we select the test functions $\mathbf{w}_\varphi = \boldsymbol{\zeta} \times \boldsymbol{\varphi}$ and $\mathbf{w}_\pi = -\rho_0 \boldsymbol{\zeta} \times \dot{\boldsymbol{\varphi}}$ to derive the angular momentum balance. Here, $\boldsymbol{\zeta} \in \mathbb{R}^3$ is an arbitrary but constant vector. Using vector calculus, the cross product $\boldsymbol{\zeta} \times \mathbf{a}$ can be expressed as a matrix-vector product $\hat{\boldsymbol{\zeta}} \mathbf{a}$ for any $\mathbf{a} \in \mathbb{R}^3$, where $\hat{\boldsymbol{\zeta}} \in \mathbb{R}^{3\times3}$ denotes the skew-symmetric matrix associated with $\boldsymbol{\zeta}$. Inserting these test functions into (W) and summing the first two equations of (W) yields

$$\begin{aligned} &\int_{\Omega_0} (-\rho_0 \boldsymbol{\zeta} \times \dot{\boldsymbol{\varphi}}) \cdot (\dot{\boldsymbol{\varphi}} - \mathbf{v}) \, \mathrm{dV} \\ &\quad + \int_{\Omega_0} (\boldsymbol{\zeta} \times \boldsymbol{\varphi}) \cdot \rho_0 \dot{\mathbf{v}} + (\hat{\boldsymbol{\zeta}} \nabla \boldsymbol{\varphi}) : (\mathbf{F}_\varphi \mathbf{S}) - (\boldsymbol{\zeta} \times \boldsymbol{\varphi}) \cdot (\bar{\mathbf{g}} + \bar{\mathbf{b}}) \, \mathrm{dV} \\ &\quad - \int_{\partial_\sigma \Omega_0} (\boldsymbol{\zeta} \times \boldsymbol{\varphi}) \cdot \bar{\mathbf{t}} \, \mathrm{dA} = 0 \,. \end{aligned} \tag{35}$$

Due to the symmetry of the second Piola-Kirchhoff stress tensor $\mathbf{S}$ and the skew-symmetry of $\hat{\boldsymbol{\zeta}}$, the term $\hat{\boldsymbol{\zeta}} : (\mathbf{F}_\varphi \mathbf{S} \nabla \boldsymbol{\varphi}^\mathrm{T})$ vanishes. Thus, expression (35) simplifies to

$$\boldsymbol{\zeta} \cdot \left[\int_{\Omega_0} \frac{\mathrm{d}}{\mathrm{dt}} (\boldsymbol{\varphi} \times \mathbf{v} \rho_0) - (\bar{\mathbf{g}} + \bar{\mathbf{b}}) \times \boldsymbol{\varphi} \, \mathrm{dV} - \int_{\partial_\sigma \Omega_0} \bar{\mathbf{t}} \times \boldsymbol{\varphi} \, \mathrm{dA} \right] = \boldsymbol{\zeta} \cdot (\dot{\mathbf{L}} - \mathbf{m}^\mathrm{ext}) = 0 \,. \tag{36}$$

Here, $\mathbf{m}^\mathrm{ext}$ denotes the external torque acting on the body and its boundary. Hence, the angular momentum is conserved iff $\mathbf{m}^\mathrm{ext} = \mathbf{0}$.

2.6. Alternative size-reduced port-Hamiltonian formulations

The present pH formulation is based on the introduction of independent strain-type fields $\{\mathbf{C}, \mathbf{G}, J\}$. Alternatively, a reduced number of independent strain-type fields may be used. For completeness, we outline the construction of size-reduced pH formulations. Since the procedure to setup the respective pH formulation closely follows the lines above, we merely sketch the main steps.

2.6.1. Size-reduced mixed port-Hamiltonian formulation based on mixed fields $\{\mathbf{G}, J\}$

In [25,26] the independent fields $\{\mathbf{G}, J\}$ are introduced, while the right Cauchy-Green tensor is directly formulated in terms of the deformation map. In particular, instead of introducing the independent field $\mathbf{C}$, $\mathbf{C}_\varphi$, which is defined in (5), is used directly. The pH formulation associated with [25,26] is based on the Hamiltonian

$$\mathcal{H}_1(\mathbf{x}_1) = \int_{\Omega_0} \left(\frac{1}{2} \rho_0 \mathbf{v} \cdot \mathbf{v} + \widetilde{\mathcal{W}}(\mathbf{C}_\varphi, \mathbf{G}, J) - \bar{\mathbf{g}} \cdot \boldsymbol{\varphi} \right) \mathrm{dV} \,, \tag{37}$$

implying the reduced set of energy variables

$$\mathbf{x}_1 = \begin{bmatrix} \boldsymbol{\varphi} \\ \mathbf{v} \\ \mathbf{G} \\ J \end{bmatrix} . \tag{38}$$

The functional derivative of Hamiltonian (37) is given by

$$\delta_{\mathbf{x}_1}\mathcal{H}_1(\mathbf{x}_1) = \begin{bmatrix} -\bar{\mathbf{g}} - \mathrm{Div}(2\mathbf{F}_\varphi \partial_{\mathbf{C}}\widetilde{\mathcal{W}}) \\ \rho_0 \mathbf{v} \\ \partial_{\mathbf{G}}\widetilde{\mathcal{W}} \\ \partial_J \widetilde{\mathcal{W}} \end{bmatrix}, \tag{39}$$

where $\widetilde{\mathcal{W}} = \widetilde{\mathcal{W}}(\mathbf{C}_\varphi, \mathbf{G}, J)$. The pH formulation of the local field equations again assumes the form (20), where the size-reduced differential operator is given by

$$\mathcal{J}_1 = \begin{bmatrix} 0 & I & 0 & 0 \\ -I & 0 & \mathrm{Div}(2\mathbf{F}_\varphi \mathbf{C}_\varphi \gg \square) & \mathrm{Div}(J_\varphi^{-1}\mathbf{F}_\varphi \mathbf{G}_\varphi \square) \\ 0 & 2\mathbf{C}_\varphi \ggg \mathrm{sym}(\mathbf{F}_\varphi^{\mathrm{T}} \nabla(\square)) & 0 & 0 \\ 0 & J_\varphi^{-1}\mathbf{G}_\varphi : \mathrm{sym}(\mathbf{F}_\varphi^{\mathrm{T}} \nabla(\square)) & 0 & 0 \end{bmatrix}. \tag{40}$$

The operator $\mathcal{E}$ takes a similar form as in (24), differing only in size due to the reduced set of energy variables.

2.6.2. Size-reduced mixed port-Hamiltonian formulation based on mixed field $\mathbf{E}$

The recently published works [16–18] rely on the introduction of the Green-Lagrangian strain tensor as an independent field. Since the Green-Lagrangian strain tensor is given by

$$\mathbf{E} = \frac{1}{2}(\mathbf{C} - \mathbf{I}), \tag{41}$$

we have $2\dot{\mathbf{E}} = \dot{\mathbf{C}}$ and we thus may use the right Cauchy-Green tensor again. Correspondingly, the Hamiltonian now assumes the form

$$\mathcal{H}_2(\mathbf{x}_2) = \int_{\Omega_0} \left(\frac{1}{2}\rho_0 \mathbf{v}\cdot\mathbf{v} + \widehat{\mathcal{W}}(\mathbf{C}) - \bar{\mathbf{g}}\cdot\boldsymbol{\varphi}\right) \mathrm{dV}, \tag{42}$$

where the stored energy $\widehat{\mathcal{W}}$ has been introduced in (9). Accordingly, the reduced set of energy variables is given by

$$\mathbf{x}_2 = \begin{bmatrix} \boldsymbol{\varphi} \\ \mathbf{v} \\ \mathbf{C} \end{bmatrix} \tag{43}$$

and the functional derivative of Hamiltonian (42) reads

$$\delta_{\mathbf{x}_2}\mathcal{H}_2(\mathbf{x}_2) = \begin{bmatrix} -\bar{\mathbf{g}} \\ \rho_0 \mathbf{v} \\ \partial_{\mathbf{C}}\widehat{\mathcal{W}} \end{bmatrix}. \tag{44}$$

The pH formulation of the local field equations again assumes the form (20), where the size-reduced differential operator is given by

$$\mathcal{J}_2 = \begin{bmatrix} 0 & I & 0 \\ -I & 0 & \mathrm{Div}(2\mathbf{F}_\varphi \square) \\ 0 & 2\,\mathrm{sym}(\mathbf{F}_\varphi^{\mathrm{T}} \nabla(\square)) & 0 \end{bmatrix}. \tag{45}$$

In analogy to Subsection 2.6.1, the operator $\mathcal{E}$ follows the same definition as in (24), differing only in its dimension.

It is worth noting that the constitutive law in [16,17] is restricted to Saint Venant-Kirchhoff material from the outset. For Saint Venant-Kirchhoff material,

$$\mathbf{S} = 2\partial_{\mathbf{C}}\widehat{\mathcal{W}} = \mathbb{C} : \mathbf{E}, \tag{46}$$

where $\mathbb{C}$ is the fourth-order elasticity tensor. Consequently, in the pH formulation the independent right Cauchy-Green tensor can be replaced with the independent second Piola-Kirchhoff stress field by using the relations $\partial_{\mathbf{C}}\widehat{\mathcal{W}} = \frac{1}{2}\mathbf{S}$ and $\dot{\mathbf{C}} = 2\dot{\mathbf{E}} = 2\mathbb{C}^{-1} : \dot{\mathbf{S}}$. We refer to[16,17] for further details of the resulting 'velocity-stress formulation'.

2.6.3. Fully size-reduced displacement-based pH formulation

In a further step one can consider a fully size-reduced displacement-based pH formulation in which the Hamiltonian is given by

$$\mathcal{H}_3(\mathbf{x}_3) = \int_{\Omega_0} \left(\frac{1}{2}\rho_0 \mathbf{v}\cdot\mathbf{v} + \widetilde{\mathcal{W}}(\mathbf{C}_\varphi, \mathbf{G}_\varphi, J_\varphi) - \bar{\mathbf{g}}\cdot\boldsymbol{\varphi}\right) \mathrm{dV}, \tag{47}$$

where the stored energy function $\widetilde{\mathcal{W}}$ has been introduced in (9). Hamiltonian (47) gives rise to the classic set of variables

$$\mathbf{x}_3 = \begin{bmatrix} \boldsymbol{\varphi} \\ \mathbf{v} \end{bmatrix} \tag{48}$$

associated with a pure displacement-based formulation. The functional derivative of the Hamiltonian (47) is then given by

$$\delta_{\mathbf{x}_3}\mathcal{H}_3(\mathbf{x}_3) = \begin{bmatrix} -\bar{\mathbf{g}} - \mathrm{Div}(2\mathbf{F}_\varphi(\partial_{\mathbf{C}}\widetilde{\mathcal{W}} + \mathbf{C}_\varphi \ggg \partial_{\mathbf{G}}\widetilde{\mathcal{W}} + \frac{1}{2}J_\varphi^{-1}\partial_J \widetilde{\mathcal{W}}\mathbf{G}_\varphi)) \\ \rho_0 \mathbf{v} \end{bmatrix}, \tag{49}$$

where $\widetilde{\mathcal{W}} = \widetilde{\mathcal{W}}(\mathbf{C}_\varphi, \mathbf{G}_\varphi, J_\varphi)$. Again, we obtain a pH formulation in the form of (20), where, however, the operator $\mathcal{J}_3$ reduces to its canonical form

$$\mathcal{J}_3 = \begin{bmatrix} 0 & I \\ -I & 0 \end{bmatrix} . \tag{50}$$

As in the previous subsections, the operator $\mathcal{E}$ follows the same definition as in (24), differing only in its dimension.

The displacement-based formulation lies at the heart of the first energy-momentum scheme for nonlinear elastodynamics devised in [19].

3. Discretization in time

In order to preserve the structural properties of the port-Hamiltonian formulation in numerical simulations, an appropriate time discretization scheme is essential. To this end, we introduce a variant of the implicit midpoint scheme, which relies on the notion of a discrete derivative. After presenting the time-discrete weak form, we show that the conservation laws are preserved under the proposed time discretization.

We begin by dividing the time interval $\mathcal{I}$ into discrete subintervals $\mathcal{I}_n = [t_n, t_{n+1}]$ for $n \in \{0, \dots, N\}$ with time-step size $\Delta t_n = t_{n+1} - t_n$. The average value of a quantity $(\bullet)(t)$ over one time interval is defined as

$$(\bullet)_{n+1/2} = \frac{1}{2}\left[(\bullet)_n + (\bullet)_{n+1}\right] , \tag{51}$$

where $(\bullet)_n = (\bullet)(t_n)$ and $(\bullet)_{n+1} = (\bullet)(t_{n+1})$. Furthermore, the time derivative $(\dot\bullet)$ is approximated using finite differences given by

$$(\dot\bullet) \approx \frac{\Delta(\bullet)_n}{\Delta t_n} = \frac{(\bullet)_{n+1} - (\bullet)_n}{\Delta t_n} . \tag{52}$$

This leads to the time-discrete counterpart of the weak form (W), given by

$$\begin{aligned}
&\int_{\Omega_0} \mathbf{w}_\pi \cdot \Big(\frac{\boldsymbol{\varphi}_{n+1} - \boldsymbol{\varphi}_n}{\Delta t_n} - \mathbf{v}_{n+1/2}\Big)\,\mathrm{dV} = 0 \\
&\int_{\Omega_0} \mathbf{w}_\varphi \cdot \rho_0 \frac{\mathbf{v}_{n+1} - \mathbf{v}_n}{\Delta t_n} + \mathrm{sym}(\mathbf{F}^{\mathrm{T}}_{\boldsymbol{\varphi}_{n+1/2}} \nabla \mathbf{w}_\varphi) : \bar{\mathbf{S}}\,\mathrm{dV} = \int_{\Omega_0} \mathbf{w}_\varphi \cdot \big(\bar{\mathbf{g}}_{n+1/2} + \bar{\mathbf{b}}_{n+1/2}\big)\,\mathrm{dV} + \int_{\partial\Omega_0} \mathbf{w}_\varphi \cdot \bar{\mathbf{t}}_{n+1/2}\,\mathrm{dA} \\
&\int_{\Omega_0} \mathbf{w}_{\mathbf{C}} : \Big[\boldsymbol{\Lambda}_{\mathbf{C}_{n+1}} - \mathrm{D}_{\mathbf{C}}\widetilde{\mathcal{W}}\Big]\,\mathrm{dV} = 0 \\
&\int_{\Omega_0} \mathbf{w}_{\mathbf{G}} : \Big[\boldsymbol{\Lambda}_{\mathbf{G}_{n+1}} - \mathrm{D}_{\mathbf{G}}\widetilde{\mathcal{W}}\Big]\,\mathrm{dV} = 0 \\
&\int_{\Omega_0} w_J \Big[\lambda_{n+1} - \mathrm{D}_J\widetilde{\mathcal{W}}\Big]\,\mathrm{dV} = 0 \\
&\int_{\Omega_0} \mathbf{w}_{\boldsymbol{\Lambda}_{\mathbf{C}}} : \Big[\frac{\mathbf{C}_{n+1} - \mathbf{C}_n}{\Delta t_n} - 2\,\mathrm{sym}(\mathbf{F}^{\mathrm{T}}_{\boldsymbol{\varphi}_{n+1/2}} \nabla \mathbf{v}_{n+1/2})\Big]\,\mathrm{dV} = 0 \\
&\int_{\Omega_0} \mathbf{w}_{\boldsymbol{\Lambda}_{\mathbf{G}}} : \Big[\frac{\mathbf{G}_{n+1} - \mathbf{G}_n}{\Delta t_n} - 2\mathbf{C}_{\boldsymbol{\varphi}_{n+1/2}} \overset{\ast}{\ast} \mathrm{sym}(\mathbf{F}^{\mathrm{T}}_{\boldsymbol{\varphi}_{n+1/2}} \nabla \mathbf{v}_{n+1/2})\Big]\,\mathrm{dV} = 0 \\
&\int_{\Omega_0} w_\lambda \Big[\frac{J_{n+1} - J_n}{\Delta t_n} - (J_{\boldsymbol{\varphi}_{n+1/2}})^{-1}\mathbf{G}_{\boldsymbol{\varphi}_{n+1/2}} : \mathrm{sym}(\mathbf{F}^{\mathrm{T}}_{\boldsymbol{\varphi}_{n+1/2}} \nabla \mathbf{v}_{n+1/2})\Big]\,\mathrm{dV} = 0 ,
\end{aligned} \tag{53}$$

where the time-discrete second Piola-Kirchhoff stress tensor $\bar{\mathbf{S}}$ is defined by

$$\bar{\mathbf{S}} = 2\boldsymbol{\Lambda}_{\mathbf{C}_{n+1}} + 2\boldsymbol{\Lambda}_{\mathbf{G}_{n+1}} \overset{\ast}{\ast} \mathbf{C}_{\boldsymbol{\varphi}_{n+1/2}} + \frac{\lambda_{n+1}}{J_{\boldsymbol{\varphi}_{n+1/2}}} \mathbf{G}_{\boldsymbol{\varphi}_{n+1/2}} . \tag{54}$$

In this time-discrete weak form, the partial derivatives of the energy density function, $\partial_{\mathcal{V}^i}\widetilde{\mathcal{W}}$ with $\mathcal{V}^i \in \{\mathbf{C}, \mathbf{G}, J\}$, are replaced by partitioned discrete derivatives $\mathrm{D}_{\mathcal{V}^i}\widetilde{\mathcal{W}}$ in the sense of [33] (cf. Example 1). An important property of discrete derivatives is the fulfillment of the so-called directionality property, which in the present case reads

$$\Delta\widetilde{\mathcal{W}}_n = \widetilde{\mathcal{W}}_{n+1} - \widetilde{\mathcal{W}}_n = \mathrm{D}_{\mathbf{C}}\widetilde{\mathcal{W}} : \Delta\mathbf{C}_n + \mathrm{D}_{\mathbf{G}}\widetilde{\mathcal{W}} : \Delta\mathbf{G}_n + \mathrm{D}_J\widetilde{\mathcal{W}}\Delta J_n . \tag{55}$$

In particular, the directionality property (55) facilitates the conservation of energy in the discrete setting.

To indicate the functional dependence of the present discrete derivatives, we occasionally write

$$\mathrm{D}_{\mathcal{V}^i}\widetilde{\mathcal{W}} = \mathrm{D}_{\mathcal{V}^i}\widetilde{\mathcal{W}}(\mathcal{V}_n, \mathcal{V}_{n+1}) , \tag{56}$$

where $\mathcal{V} = (\mathbf{C}, \mathbf{G}, J)$.

Moreover, in the limit $\Delta\mathcal{V}^i_n \to 0$, the discrete derivatives coincide with the derivatives of the classical midpoint rule, that is,

$$\lim_{\Delta\mathcal{V}^i_n \to 0} \Big(\mathrm{D}_{\mathcal{V}^i}\widetilde{\mathcal{W}}\Big) = \partial_{\mathcal{V}^i}\widetilde{\mathcal{W}}|_{\mathcal{V}_{n+1/2}} . \tag{57}$$

Example 1. Consider a separable stored energy function of the form

$$\widetilde{\mathcal{W}}(\mathbf{C},\mathbf{G},J)=\widetilde{\mathcal{W}}_1(\mathbf{C})+\widetilde{\mathcal{W}}_2(\mathbf{G})+\widetilde{\mathcal{W}}_3(J) \tag{58}$$

and assume that the functions $\widetilde{\mathcal{W}}_1(\mathbf{C})$ and $\widetilde{\mathcal{W}}_2(\mathbf{G})$ are at most quadratic, while $\widetilde{\mathcal{W}}_3(J)$ is a general nonlinear function. Then the partitioned discrete derivatives $\mathrm{D}_{\mathcal{Y}^i}\widetilde{\mathcal{W}}$ are given by

$$\begin{aligned}
\mathrm{D}_{\mathbf{C}}\widetilde{\mathcal{W}} &= \partial_{\mathbf{C}}\widetilde{\mathcal{W}}(\mathbf{C}_{n+1/2})\\
\mathrm{D}_{\mathbf{G}}\widetilde{\mathcal{W}} &= \partial_{\mathbf{G}}\widetilde{\mathcal{W}}(\mathbf{G}_{n+1/2})\\
\mathrm{D}_{J}\widetilde{\mathcal{W}} &= \frac{\widetilde{\mathcal{W}}_3(J_{n+1})-\widetilde{\mathcal{W}}_3(J_n)}{J_{n+1}-J_n}\,,
\end{aligned} \tag{59}$$

where $\mathrm{D}_J\widetilde{\mathcal{W}}$ is known as the Greenspan formula [34].

3.1. Time-discrete conservation of energy

A system conserves energy in the time-discrete setting if the difference in the Hamiltonian $\mathcal{H}$ between two time steps vanishes, that is,

$$\mathcal{H}_{n+1}-\mathcal{H}_n=\Delta\mathcal{H}_n=0 \tag{60}$$

for each time step Δt_n, where

$$\Delta\mathcal{H}_n=\int_{\Omega_0}\Delta T_n+\Delta\widetilde{\mathcal{W}}_n+\Delta V_n\,\mathrm{dV}\,. \tag{61}$$

In the last equation, $T=\frac{1}{2}\rho_0\mathbf{v}\cdot\mathbf{v}$ and $V=-\bar{\mathbf{g}}\cdot\boldsymbol{\varphi}$. To prove energy conservation, we start from the time-discrete weak form, given in (53). Similarly to Section 2.5.1, we select admissible time-discrete test functions $\mathbf{w}_\varphi=\Delta\boldsymbol{\varphi}_n/\Delta t_n$, $\mathbf{w}_\pi=-\rho_0\Delta\mathbf{v}_n/\Delta t_n$, $\mathbf{w}_C=-\Delta\mathbf{C}_n/\Delta t_n$, $\mathbf{w}_G=-\Delta\mathbf{G}_n/\Delta t_n$, $w_J=-\Delta J_n/\Delta t_n$, $\mathbf{w}_{\boldsymbol{\Lambda}_\mathbf{C}}=\boldsymbol{\Lambda}_{\mathbf{C}_{n+1}}$, $\mathbf{w}_{\boldsymbol{\Lambda}_\mathbf{G}}=\boldsymbol{\Lambda}_{\mathbf{G}_{n+1}}$ and $w_\lambda=\lambda_{n+1}$. Inserting these into the weak form (53) and summing the equations yields

$$\begin{aligned}
&\int_{\Omega_0}\mathbf{v}_{n+1/2}\cdot\frac{\rho_0}{\Delta t_n}\big(\mathbf{v}_{n+1}-\mathbf{v}_n\big)+\frac{\Delta\mathbf{C}_n}{\Delta t_n}:\mathrm{D}_{\mathbf{C}}\widetilde{\mathcal{W}}+\frac{\Delta\mathbf{G}_n}{\Delta t_n}:\mathrm{D}_{\mathbf{G}}\widetilde{\mathcal{W}}+\frac{\Delta J_n}{\Delta t_n}\mathrm{D}_J\widetilde{\mathcal{W}}\,\mathrm{dV}\\
&\quad-\int_{\Omega_0}\frac{\Delta\boldsymbol{\varphi}_n}{\Delta t_n}\cdot\big(\bar{\mathbf{g}}_{n+1/2}+\bar{\mathbf{b}}_{n+1/2}\big)\,\mathrm{dV}-\int_{\partial\Omega_0}\frac{\Delta\varphi_\mathrm{n}}{\Delta\mathrm{t_n}}\cdot\bar{\mathbf{t}}_{\mathrm{n}+1/2}\,\mathrm{dA}=0\,,
\end{aligned} \tag{62}$$

which coincides with (60) iff $\bar{\mathbf{t}}_{n+1/2}=\mathbf{0}$ and $\bar{\mathbf{b}}_{n+1/2}=\mathbf{0}$. Note that the relation $\Delta\boldsymbol{\varphi}_n=\Delta t_n\mathbf{v}_{n+1/2}$ was used to obtain (62).

3.2. Time-discrete conservation of angular momentum

Following the approach in Section 2.5.2, we choose the time-discrete test functions $\mathbf{w}_\varphi=\boldsymbol{\zeta}\times\boldsymbol{\varphi}_{n+1/2}$ and $\mathbf{w}_\pi=-\rho_0\boldsymbol{\zeta}\times\frac{\Delta\boldsymbol{\varphi}_n}{\Delta t_n}$ where again $\boldsymbol{\zeta}\in\mathbb{R}^3$ is an arbitrary but constant vector. Inserting these into (53) and summing the first two equations then yields

$$\begin{aligned}
&\int_{\Omega_0}(-\rho_0\boldsymbol{\zeta}\times\Delta\boldsymbol{\varphi}_n)\cdot\Big(\frac{\Delta\boldsymbol{\varphi}_n}{\Delta t_n}-\mathbf{v}_{n+1/2}\Big)\,\mathrm{dV}+\int_{\Omega_0}(\boldsymbol{\zeta}\times\boldsymbol{\varphi}_{\mathrm{n}+1/2})\cdot\rho_0\frac{\Delta\mathbf{v}_\mathrm{n}}{\Delta\mathrm{t_n}}+(\hat{\boldsymbol{\zeta}}\nabla\boldsymbol{\varphi}_{\mathrm{n}+1/2}):(\mathbf{F}_{\varphi_{\mathrm{n}+1/2}}\bar{\mathbf{S}})\,\mathrm{dV}\\
&\quad-\int_{\Omega_0}(\boldsymbol{\zeta}\times\boldsymbol{\varphi}_{n+1/2})\cdot\big(\bar{\mathbf{g}}_{n+1/2}+\bar{\mathbf{b}}_{n+1/2}\big)\,\mathrm{dV}-\int_{\partial_\sigma\Omega_0}(\boldsymbol{\zeta}\times\boldsymbol{\varphi}_{\mathrm{n}+1/2})\cdot\bar{\mathbf{t}}_{\mathrm{n}+1/2}\,\mathrm{dA}=0\,.
\end{aligned} \tag{63}$$

Due to the symmetry of the time-discrete second Piola-Kirchhoff stress tensor $\bar{\mathbf{S}}$, the scalar product of $(\nabla\boldsymbol{\varphi}^{\mathrm{T}}_{n+1/2}\hat{\boldsymbol{\zeta}}\mathbf{F}_{n+1/2}):\bar{\mathbf{S}}$ vanishes again. With some additional vector calculus, the last equation simplifies to

$$\boldsymbol{\zeta}\cdot\left[\int_{\Omega_0}\frac{1}{\Delta t_n}\rho_0\big(\boldsymbol{\varphi}_{n+1}\times\mathbf{v}_{n+1}-\boldsymbol{\varphi}_n\times\mathbf{v}_n\big)-\big(\bar{\mathbf{g}}_{n+1/2}+\bar{\mathbf{b}}_{n+1/2}\big)\times\boldsymbol{\varphi}_{n+1/2}\,\mathrm{dV}-\int_{\partial_\sigma\Omega_0}\bar{\mathbf{t}}_{\mathrm{n}+1/2}\times\boldsymbol{\varphi}_{\mathrm{n}+1/2}\,\mathrm{dA}\right]=\boldsymbol{\zeta}\cdot\Big(\frac{\Delta\mathbf{L}_n}{\Delta t_n}-\mathbf{m}^{\mathrm{ext}}_{n+1/2}\Big)=0\,. \tag{64}$$

Hence, the angular momentum is conserved in the sense that $\mathbf{L}_{n+1}=\mathbf{L}_n$ iff the time-discrete external torque $\mathbf{m}^{\mathrm{ext}}_{n+1/2}$ vanishes.

4. Discretization in space

This section addresses the spatial discretization of the fully mixed formulation. Furthermore, it is shown that the resulting space-discrete weak form can be recast as a discrete port-Hamiltonian system.

4.1. Approximation of the test and trial functions

Similarly to Section 3, we consider the weak form of the fully mixed formulation given in (W). In a first step, finite element approximations of the test and trial functions are introduced in order to discretize the governing equations in space in the framework of the Bubnov-Galerkin method.

For this purpose, we employ a standard isoparametric finite element concept as described, for example, in [35]. First, the finite element approximation of the deformation field $\boldsymbol{\varphi}$ is specified by

$$\boldsymbol{\varphi}^{\mathrm{h}} = \sum_{K=1}^{n_{\mathrm{node}}} N_{\varphi}^{K} \hat{\boldsymbol{\varphi}}^{K} = \mathbf{N}_{\varphi} \hat{\boldsymbol{\varphi}} \tag{65}$$

with

$$\begin{aligned} \hat{\boldsymbol{\varphi}} &= \begin{bmatrix} \hat{\varphi}_x^1 & \hat{\varphi}_y^1 & \hat{\varphi}_z^1 & \cdots & \hat{\varphi}_x^{n_{\mathrm{node}}} & \hat{\varphi}_y^{n_{\mathrm{node}}} & \hat{\varphi}_z^{n_{\mathrm{node}}} \end{bmatrix}^{\mathrm{T}} \in \mathbb{R}^{3n_{\mathrm{node}}} , \\ \mathbf{N}_{\varphi} &= \begin{bmatrix} N_{\varphi}^1 \mathbf{I} & \cdots & N_{\varphi}^{n_{\mathrm{node}}} \mathbf{I} \end{bmatrix} \in \mathbb{R}^{3\times 3n_{\mathrm{node}}} , \end{aligned} \tag{66}$$

where N_{φ}^{K} are Lagrangian shape functions and $K = 1, \dots, n_{\mathrm{node}}$ are n_{node} nodal points per element. The nodal position vectors $\hat{\boldsymbol{\varphi}}^{K}$ are summarized in the vector $\hat{\boldsymbol{\varphi}}$. Similarly, the shape functions are collected in the matrix $\mathbf{N}_{\varphi}$. Using standard finite element assembly procedures, we obtain a globally continuous discrete deformation field.

Similarly, the approximation of the velocity field $\mathbf{v}$ and the test functions $\{\mathbf{w}_{\varphi}, \mathbf{w}_{\pi}\}$ is given by

$$\begin{aligned} \mathbf{w}_{\varphi}^{\mathrm{h}} &= \sum_{K=1}^{n_{\mathrm{node}}} N_{\varphi}^{K} \hat{\mathbf{w}}_{\varphi}^{K} = \mathbf{N}_{\varphi} \hat{\mathbf{w}}_{\varphi} , \\ \mathbf{v}^{\mathrm{h}} &= \sum_{K=1}^{n_{\mathrm{node}}} N_{\varphi}^{K} \hat{\mathbf{v}}^{K} = \mathbf{N}_{\varphi} \hat{\mathbf{v}} , \\ \mathbf{w}_{\pi}^{\mathrm{h}} &= \sum_{K=1}^{n_{\mathrm{node}}} N_{\varphi}^{K} \hat{\mathbf{w}}_{\pi}^{K} = \mathbf{N}_{\varphi} \hat{\mathbf{w}}_{\pi} . \end{aligned} \tag{67}$$

For the tensor-valued mixed quantities $\{\mathbf{C}, \mathbf{G}\}$, their Lagrange multipliers $\{\boldsymbol{\Lambda}_{\mathbf{C}}, \boldsymbol{\Lambda}_{\mathbf{G}}\}$ and the corresponding test functions $\left\{\mathbf{w}_{\mathbf{C}}, \mathbf{w}_{\mathbf{G}}, \mathbf{w}_{\boldsymbol{\Lambda}_{\mathbf{C}}}, \mathbf{w}_{\boldsymbol{\Lambda}_{\mathbf{G}}}\right\}$, we make use of the Voigt notation to obtain an easier implementation. We differentiate between stress-related and strain-related quantities. For a symmetric stress-like second-order tensor $\mathbf{A} = \mathbf{A}^{\mathrm{T}}$ and a symmetric strain-like second-order tensor $\mathbf{B} = \mathbf{B}^{\mathrm{T}}$, the Voigt notation is defined as

$$\begin{aligned} \{\mathbf{A}\}_{\mathrm{V}} &= \begin{bmatrix} A_{11} & A_{22} & A_{33} & A_{12} & A_{23} & A_{13} \end{bmatrix}^{\mathrm{T}} , \\ \{\mathbf{B}\}_{\mathrm{V}} &= \begin{bmatrix} B_{11} & B_{22} & B_{33} & 2B_{12} & 2B_{23} & 2B_{13} \end{bmatrix}^{\mathrm{T}} , \end{aligned} \tag{68}$$

respectively. With this in mind, we next provide the finite element approximations of the mixed fields, which do not require inter-element continuity. In fact, we focus on approximations of the mixed fields which are discontinuous across element boundaries. This way, static condensation can be applied to eliminate the corresponding local degrees of freedom on element level, see Section 5 for further details. The approximation of the right Cauchy-Green deformation tensor $\mathbf{C}$ is given by

$$\begin{aligned} \mathbf{C}^{\mathrm{h}} &= \sum_{L=1}^{m_{\mathrm{node}}} N_{C}^{L} \hat{\mathbf{C}}^{L} , \\ \left\{\mathbf{C}^{\mathrm{h}}\right\}_{\mathrm{V}} &= \mathbf{N}_{C} \left\{\hat{\mathbf{C}}\right\}_{\mathrm{V}} , \end{aligned} \tag{69}$$

where

$$\begin{aligned} \left\{\hat{\mathbf{C}}\right\}_{\mathrm{V}} &= \left[\left\{\hat{\mathbf{C}}^1\right\}_{\mathrm{V}}^{\mathrm{T}} \quad \cdots \quad \left\{\hat{\mathbf{C}}^{m_{\mathrm{node}}}\right\}_{\mathrm{V}}^{\mathrm{T}} \right]^{\mathrm{T}} \in \mathbb{R}^{6m_{\mathrm{node}}} , \\ \mathbf{N}_{C} &= \begin{bmatrix} N_{C}^1 \mathbf{I}_6 & \cdots & N_{C}^{m_{\mathrm{node}}} \mathbf{I}_6 \end{bmatrix} \in \mathbb{R}^{6\times 6m_{\mathrm{node}}} . \end{aligned} \tag{70}$$

Here, m_{node} shape functions N_{C}^{L} are used per element. Furthermore, $\mathbf{I}_6$ is the identity matrix in $\mathbb{R}^{6\times 6}$. Note that although $\mathbf{C}^{\mathrm{h}}$ is defined only on a single element e, a superscript e is omitted here for the sake of readability.

Similarly, for the remaining matrix-valued mixed fields, we define

$$\begin{aligned} &\left\{\mathbf{G}^{\mathrm{h}}\right\}_{\mathrm{V}} = \mathbf{N}_{C} \left\{\hat{\mathbf{G}}\right\}_{\mathrm{V}} , \quad \left\{\boldsymbol{\Lambda}_{\mathbf{C}}^{\mathrm{h}}\right\}_{\mathrm{V}} = \mathbf{N}_{C} \left\{\hat{\boldsymbol{\Lambda}}_{\mathbf{C}}\right\}_{\mathrm{V}} , \quad \left\{\boldsymbol{\Lambda}_{\mathbf{G}}^{\mathrm{h}}\right\}_{\mathrm{V}} = \mathbf{N}_{C} \left\{\hat{\boldsymbol{\Lambda}}_{\mathbf{G}}\right\}_{\mathrm{V}} , \\ &\left\{\mathbf{w}_{\mathbf{C}}^{\mathrm{h}}\right\}_{\mathrm{V}} = \mathbf{N}_{C} \left\{\hat{\mathbf{w}}_{\mathbf{C}}\right\}_{\mathrm{V}} , \quad \left\{\mathbf{w}_{\mathbf{G}}^{\mathrm{h}}\right\}_{\mathrm{V}} = \mathbf{N}_{C} \left\{\hat{\mathbf{w}}_{\mathbf{G}}\right\}_{\mathrm{V}} , \quad \left\{\mathbf{w}_{\boldsymbol{\Lambda}_{\mathbf{C}}}^{\mathrm{h}}\right\}_{\mathrm{V}} = \mathbf{N}_{C} \left\{\hat{\mathbf{w}}_{\boldsymbol{\Lambda}_{\mathbf{C}}}\right\}_{\mathrm{V}} , \quad \left\{\mathbf{w}_{\boldsymbol{\Lambda}_{\mathbf{G}}}^{\mathrm{h}}\right\}_{\mathrm{V}} = \mathbf{N}_{C} \left\{\hat{\mathbf{w}}_{\boldsymbol{\Lambda}_{\mathbf{G}}}\right\}_{\mathrm{V}} . \end{aligned} \tag{71}$$

Lastly, the remaining mixed fields $\{J, \lambda\}$ and the corresponding test functions $\{w_J, w_{\lambda}\}$ are discretized with shape functions N_{J}^{I}, where no Voigt notation is necessary. Consequently, we introduce

$$J^{\mathrm{h}} = \sum_{I=1}^{p_{\mathrm{node}}} N_{J}^{I} \hat{J}^{I} = \mathbf{N}_{J} \hat{\mathbf{J}} , \tag{72}$$

where

$$\begin{aligned}\hat{\mathbf{J}} &= \begin{bmatrix}\hat{J}^1 & \cdots & \hat{J}^{p_{\text{node}}}\end{bmatrix}^{\mathrm{T}} \in \mathbb{R}^{p_{\text{node}}}\,,\\ \mathbf{N}_J &= \begin{bmatrix}N_J^1 & \cdots & N_J^{p_{\text{node}}}\end{bmatrix} \in \mathbb{R}^{p_{\text{node}}}\end{aligned} \tag{73}$$

as well as

$$w_J^{\mathrm{h}} = \mathbf{N}_J \hat{\mathbf{w}}_J\,, \quad \lambda^{\mathrm{h}} = \mathbf{N}_J \hat{\boldsymbol{\lambda}}, \quad w_\lambda^{\mathrm{h}} = \mathbf{N}_J \hat{\mathbf{w}}_\lambda\,. \tag{74}$$

Based on the stored energy $\widetilde{\mathcal{W}}$, we define the stored energy functional

$$\mathcal{U} = \int_{\Omega_0} \widetilde{\mathcal{W}}(\mathbf{C}, \mathbf{G}, J)\,\mathrm{dV}\,. \tag{75}$$

Inserting the space-discrete versions of $\mathbf{C}$, $\mathbf{G}$ and J, we obtain the discretized stored energy functional

$$\mathcal{U}^{\mathrm{h}} := \int_{\Omega_0} \widetilde{\mathcal{W}}^{\mathrm{h}}\,\mathrm{dV} = \int_{\Omega_0} \widetilde{\mathcal{W}}(\mathbf{C}^{\mathrm{h}}, \mathbf{G}^{\mathrm{h}}, \mathrm{J}^{\mathrm{h}})\,\mathrm{dV} = \int_{\Omega_0} \widetilde{\mathcal{W}}(\mathrm{N}_{\mathrm{C}}^{\mathrm{L}}\hat{\mathbf{C}}^{\mathrm{L}}, \mathrm{N}_{\mathrm{C}}^{\mathrm{L}}\hat{\mathbf{G}}^{\mathrm{L}}, \mathrm{N}_{\mathrm{J}}^{\mathrm{I}}\hat{\mathrm{J}}^{\mathrm{I}})\,\mathrm{dV} =: \mathrm{U}\big(\{\hat{\mathbf{C}}\}_{\mathrm{V}}, \{\hat{\mathbf{G}}\}_{\mathrm{V}}, \hat{\mathbf{J}}\big)\,, \tag{76}$$

where Einstein's summation convention is applied to the arguments of the function $\widetilde{\mathcal{W}}$. Taking the time derivative and applying the chain rule yields

$$\begin{aligned}\frac{\mathrm{d}}{\mathrm{dt}}U &= \int_{\Omega_0} \partial_{\mathbf{C}}\widetilde{\mathcal{W}}^{\mathrm{h}} : \frac{\mathrm{d}}{\mathrm{dt}}\big(N_C^L\hat{\mathbf{C}}^L\big) + \partial_{\mathbf{G}}\widetilde{\mathcal{W}}^{\mathrm{h}} : \frac{\mathrm{d}}{\mathrm{dt}}\big(N_C^L\hat{\mathbf{G}}^L\big) + \partial_J\widetilde{\mathcal{W}}^{\mathrm{h}}\frac{\mathrm{d}}{\mathrm{dt}}\big(N_J^I\hat{J}^I\big)\,\mathrm{dV}\\ &= \Big\{\dot{\hat{\mathbf{C}}}\Big\}_{\mathrm{V}}^{\mathrm{T}}\int_{\Omega_0}\mathbf{N}_{\mathrm{C}}^{\mathrm{T}}\Big\{\partial_{\mathbf{C}}\widetilde{\mathcal{W}}^{\mathrm{h}}\Big\}_{\mathrm{V}}\,\mathrm{dV} + \Big\{\dot{\hat{\mathbf{G}}}\Big\}_{\mathrm{V}}^{\mathrm{T}}\int_{\Omega_0}\mathbf{N}_{\mathrm{C}}^{\mathrm{T}}\Big\{\partial_{\mathbf{G}}\widetilde{\mathcal{W}}^{\mathrm{h}}\Big\}_{\mathrm{V}}\,\mathrm{dV} + \dot{\hat{\mathbf{J}}}^{\mathrm{T}}\int_{\Omega_0}\mathbf{N}_{\mathrm{J}}^{\mathrm{T}}\partial_{\mathrm{J}}\widetilde{\mathcal{W}}^{\mathrm{h}}\,\mathrm{dV}\,.\end{aligned} \tag{77}$$

Consequently, the partial derivatives of the discrete stored energy function U defined in (76) are given by

$$\begin{aligned}\partial_{\hat{\mathbf{C}}}U &= \int_{\Omega_0}\mathbf{N}_C^{\mathrm{T}}\Big\{\partial_{\mathbf{C}}\widetilde{\mathcal{W}}^{\mathrm{h}}\Big\}_{\mathrm{V}}\,\mathrm{dV}\,,\\ \partial_{\hat{\mathbf{G}}}U &= \int_{\Omega_0}\mathbf{N}_C^{\mathrm{T}}\Big\{\partial_{\mathbf{G}}\widetilde{\mathcal{W}}^{\mathrm{h}}\Big\}_{\mathrm{V}}\,\mathrm{dV}\,,\\ \partial_J U &= \int_{\Omega_0}\mathbf{N}_J^{\mathrm{T}}\partial_J\widetilde{\mathcal{W}}^{\mathrm{h}}\,\mathrm{dV}\,.\end{aligned} \tag{78}$$

To avoid clumsy notation, $\partial_{\hat{\mathbf{C}}}U$ and $\partial_{\hat{\mathbf{G}}}U$ represent $\partial U/\partial\{\hat{\mathbf{C}}\}_{\mathrm{V}}$ and $\partial U/\partial\{\hat{\mathbf{G}}\}_{\mathrm{V}}$. Taking into account the above approximations of the test and trial functions, weak form (W) can be written as

$$\begin{aligned}&\int_{\Omega_0}\mathbf{w}_\pi^{\mathrm{h}}\cdot(\dot{\boldsymbol{\varphi}}^{\mathrm{h}} - \mathbf{v}^{\mathrm{h}})\,\mathrm{dV} = 0\\ &\int_{\Omega_0}\mathbf{w}_\varphi^{\mathrm{h}}\cdot\rho_0\dot{\mathbf{v}}^{\mathrm{h}} + 2\,\mathrm{sym}(\mathbf{F}_{\boldsymbol{\varphi}^{\mathrm{h}}}^{\mathrm{T}}\nabla\mathbf{w}_\varphi^{\mathrm{h}}) : \Big(\boldsymbol{\Lambda}_{\mathbf{C}}^{\mathrm{h}} + \boldsymbol{\Lambda}_{\mathbf{G}}^{\mathrm{h}} \lll \mathbf{C}_{\boldsymbol{\varphi}^{\mathrm{h}}} + \frac{\lambda^{\mathrm{h}}}{2J_{\boldsymbol{\varphi}^{\mathrm{h}}}}\mathbf{G}_{\boldsymbol{\varphi}^{\mathrm{h}}}\Big)\,\mathrm{dV} = \int_{\Omega_0}\mathbf{w}_\varphi^{\mathrm{h}}\cdot\big(\bar{\mathbf{g}} + \bar{\mathbf{b}}\big)\,\mathrm{dV} + \int_{\partial\Omega_0}\mathbf{w}_\varphi^{\mathrm{h}}\cdot\bar{\mathbf{t}}\,\mathrm{dA}\\ &\int_{\Omega_0}\mathbf{w}_{\mathbf{C}}^{\mathrm{h}} : \Big[\boldsymbol{\Lambda}_{\mathbf{C}}^{\mathrm{h}} - \partial_{\mathbf{C}}\widetilde{\mathcal{W}}^{\mathrm{h}}\Big]\,\mathrm{dV} = 0\\ &\int_{\Omega_0}\mathbf{w}_{\mathbf{G}}^{\mathrm{h}} : \Big[\boldsymbol{\Lambda}_{\mathbf{G}}^{\mathrm{h}} - \partial_{\mathbf{G}}\widetilde{\mathcal{W}}^{\mathrm{h}}\Big]\,\mathrm{dV} = 0\\ &\int_{\Omega_0}w_J^{\mathrm{h}}\Big[\lambda^{\mathrm{h}} - \partial_J\widetilde{\mathcal{W}}^{\mathrm{h}}\Big]\,\mathrm{dV} = 0\\ &\int_{\Omega_0}\mathbf{w}_{\boldsymbol{\Lambda}_{\mathbf{C}}}^{\mathrm{h}} : \Big[\dot{\mathbf{C}}^{\mathrm{h}} - 2\,\mathrm{sym}(\mathbf{F}_{\boldsymbol{\varphi}^{\mathrm{h}}}^{\mathrm{T}}\nabla\mathbf{v}^{\mathrm{h}})\Big]\,\mathrm{dV} = 0\\ &\int_{\Omega_0}\mathbf{w}_{\boldsymbol{\Lambda}_{\mathbf{G}}}^{\mathrm{h}} : \Big[\dot{\mathbf{G}}^{\mathrm{h}} - 2\mathbf{C}_{\boldsymbol{\varphi}^{\mathrm{h}}} \lll \mathrm{sym}(\mathbf{F}_{\boldsymbol{\varphi}^{\mathrm{h}}}^{\mathrm{T}}\nabla\mathbf{v}^{\mathrm{h}})\Big]\,\mathrm{dV} = 0\\ &\int_{\Omega_0}w_\lambda^{\mathrm{h}}\Big[\dot{J}^{\mathrm{h}} - J_{\boldsymbol{\varphi}^{\mathrm{h}}}^{-1}\mathbf{G}_{\boldsymbol{\varphi}^{\mathrm{h}}} : \mathrm{sym}(\mathbf{F}_{\boldsymbol{\varphi}^{\mathrm{h}}}^{\mathrm{T}}\nabla\mathbf{v}^{\mathrm{h}})\Big]\,\mathrm{dV} = 0\,.\end{aligned} \tag{79}$$

Inserting the specific finite element approximations into (79), we obtain the following system of equations

$$\begin{aligned}
\dot{\hat{\boldsymbol{\varphi}}} - \hat{\mathbf{v}} &= \mathbf{0} \\
\hat{\mathbf{w}}_{\varphi}^{\mathrm{T}}\left[\mathbf{M}_{\varphi}^{\rho}\dot{\hat{\mathbf{v}}} + \boldsymbol{\Phi}(\hat{\boldsymbol{\varphi}})\left\{\hat{\boldsymbol{\Lambda}}_{\mathbf{C}}\right\}_{\mathrm{V}} + \boldsymbol{\Psi}(\hat{\boldsymbol{\varphi}})\left\{\hat{\boldsymbol{\Lambda}}_{\mathbf{G}}\right\}_{\mathrm{V}} + \boldsymbol{\Xi}(\hat{\boldsymbol{\varphi}})\hat{\boldsymbol{\lambda}} - \mathbf{g} - \mathbf{b} - \mathbf{t}\right] &= 0 \\
\{\hat{\mathbf{w}}_{\mathbf{C}}\}_{\mathrm{V}}^{\mathrm{T}}\left[\mathbf{M}_{\mathbf{C}}\left\{\hat{\boldsymbol{\Lambda}}_{\mathbf{C}}\right\}_{\mathrm{V}} - \partial_{\hat{\mathbf{C}}}U\right] &= 0 \\
\{\hat{\mathbf{w}}_{\mathbf{G}}\}_{\mathrm{V}}^{\mathrm{T}}\left[\mathbf{M}_{\mathbf{C}}\left\{\hat{\boldsymbol{\Lambda}}_{\mathbf{G}}\right\}_{\mathrm{V}} - \partial_{\hat{\mathbf{G}}}U\right] &= 0 \\
\hat{\mathbf{w}}_{J}^{\mathrm{T}}\left[\mathbf{M}_{J}\hat{\boldsymbol{\lambda}} - \partial_{J}U\right] &= 0 \\
\left\{\hat{\mathbf{w}}_{\boldsymbol{\Lambda}_{\mathbf{C}}}\right\}_{\mathrm{V}}^{\mathrm{T}}\left[\mathbf{M}_{\mathbf{C}}\left\{\dot{\hat{\mathbf{C}}}\right\}_{\mathrm{V}} - \boldsymbol{\Phi}^{\mathrm{T}}(\hat{\boldsymbol{\varphi}})\hat{\mathbf{v}}\right] &= 0 \\
\left\{\hat{\mathbf{w}}_{\boldsymbol{\Lambda}_{\mathbf{G}}}\right\}_{\mathrm{V}}^{\mathrm{T}}\left[\mathbf{M}_{\mathbf{C}}\left\{\dot{\hat{\mathbf{G}}}\right\}_{\mathrm{V}} - \boldsymbol{\Psi}^{\mathrm{T}}(\hat{\boldsymbol{\varphi}})\hat{\mathbf{v}}\right] &= 0 \\
\hat{\mathbf{w}}_{\lambda}^{\mathrm{T}}\left[\mathbf{M}_{J}\dot{\hat{\mathbf{J}}} - \boldsymbol{\Xi}^{\mathrm{T}}(\hat{\boldsymbol{\varphi}})\hat{\mathbf{v}}\right] &= 0\,.
\end{aligned} \tag{80}$$

Here, the matrices $\left\{\mathbf{M}_{\varphi}^{\rho}, \mathbf{M}_{\mathbf{C}}, \mathbf{M}_{J}\right\}$ and $\{\boldsymbol{\Phi}(\hat{\boldsymbol{\varphi}}), \boldsymbol{\Psi}(\hat{\boldsymbol{\varphi}}), \boldsymbol{\Xi}(\hat{\boldsymbol{\varphi}}), \mathbf{g}, \mathbf{b}, \mathbf{t}\}$ are defined as

$$\begin{aligned}
&\mathbf{M}_{\varphi}^{\rho} = \int_{\Omega_0} \rho_0 \mathbf{N}_{\varphi}^{\mathrm{T}}\mathbf{N}_{\varphi}\,\mathrm{dV}\,, \quad \mathbf{M}_{\mathbf{C}} = \int_{\Omega_0} \mathbf{N}_{\mathrm{C}}^{\mathrm{T}}\mathbf{N}_{\mathrm{C}}\,\mathrm{dV}\,, \quad \mathbf{M}_{\mathrm{J}} = \int_{\Omega_0} \mathbf{N}_{\mathrm{J}}^{\mathrm{T}}\mathbf{N}_{\mathrm{J}}\,\mathrm{dV}\,, \\
&\boldsymbol{\Phi}(\hat{\boldsymbol{\varphi}}) = \int_{\Omega_0} 2\mathbb{B}_{\hat{\boldsymbol{\varphi}}}^{\mathrm{T}}\mathbf{N}_{\mathrm{C}}\,\mathrm{dV}\,, \quad \boldsymbol{\Psi}(\hat{\boldsymbol{\varphi}}) = \int_{\Omega_0} 2\mathbb{B}_{\hat{\boldsymbol{\varphi}}}^{\mathrm{T}} D(\mathbf{C}_{\varphi^{\mathrm{h}}})\mathbf{N}_{\mathrm{C}}\,\mathrm{dV}\,, \quad \boldsymbol{\Xi}(\hat{\boldsymbol{\varphi}}) = \int_{\Omega_0} \mathbb{B}_{\hat{\boldsymbol{\varphi}}}^{\mathrm{T}} \mathrm{J}_{\varphi^{\mathrm{h}}}^{-1}\left\{\mathbf{G}_{\varphi^{\mathrm{h}}}\right\}_{\mathrm{V}}\mathbf{N}_{\mathrm{J}}\,\mathrm{dV}\,, \\
&\mathbf{g} = \int_{\Omega_0} \mathbf{N}_{\varphi}^{\mathrm{T}}\bar{\mathbf{g}}\,\mathrm{dV}\,, \quad \mathbf{b} = \int_{\Omega_0} \mathbf{N}_{\varphi}^{\mathrm{T}}\bar{\mathbf{b}}\,\mathrm{dV}\,, \quad \mathbf{t} = \int_{\partial\Omega_0} \mathbf{N}_{\varphi}^{\mathrm{T}}\bar{\mathbf{t}}\,\mathrm{dA}\,.
\end{aligned} \tag{81}$$

Within these definitions, $\mathbb{B}_{\hat{\boldsymbol{\varphi}}} \in \mathbb{R}^{6\times 3n_{\mathrm{node}}}$ is the classic nodal operator matrix defined through

$$\mathrm{sym}(\mathbf{F}_{\boldsymbol{\varphi}^{\mathrm{h}}}^{\mathrm{T}}\nabla\mathbf{w}_{\varphi}^{\mathrm{h}}) : \mathbf{A} = \{\mathbf{A}\}_{\mathrm{V}}^{\mathrm{T}}\mathbb{B}_{\hat{\boldsymbol{\varphi}}}\hat{\mathbf{w}}_{\varphi}\,. \tag{82}$$

For completeness, the nodal operator matrix is contained in Appendix A.1.

The matrix $D(\square) \in \mathbb{R}^{6\times 6}$ corresponds to the Voigt notation of the tensor cross product that fulfills the following relationship

$$(\mathbf{O} \divideontimes \mathbf{P}) : \mathbf{Q} = \{\mathbf{O}\}_{\mathrm{V}}^{\mathrm{T}} D(\mathbf{Q})\{\mathbf{P}\}_{\mathrm{V}}\,, \tag{83}$$

where $\mathbf{O}$ is a symmetric strain-like second-order tensor and $\mathbf{P}$ is a symmetric stress-like second-order tensor. An explicit representation of $D(\square)$ can be found in Appendix A.2.

4.2. Space-discrete formulation as discrete port-Hamiltonian system

We next show that the space-discrete formulation emanating from (80) can be brought into the form of a discrete pH system. To this end, we take into account the arbitrariness of the nodal values pertaining to the discrete test functions and perform a static condensation of the Lagrange multipliers $\left\{\hat{\boldsymbol{\Lambda}}_{\mathbf{C}}\right\}_{\mathrm{V}}$, $\left\{\hat{\boldsymbol{\Lambda}}_{\mathbf{G}}\right\}_{\mathrm{V}}$ and $\hat{\boldsymbol{\lambda}}$ on element level. Correspondingly,

$$\begin{aligned}
\left\{\hat{\boldsymbol{\Lambda}}_{\mathbf{C}}\right\}_{\mathrm{V}} &= \mathbf{M}_{\mathbf{C}}^{-1}\partial_{\hat{\mathbf{C}}}U\,, \\
\left\{\hat{\boldsymbol{\Lambda}}_{\mathbf{G}}\right\}_{\mathrm{V}} &= \mathbf{M}_{\mathbf{C}}^{-1}\partial_{\hat{\mathbf{G}}}U\,, \\
\hat{\boldsymbol{\lambda}} &= \mathbf{M}_{J}^{-1}\partial_{J}U\,,
\end{aligned} \tag{84}$$

and (80) can be recast in the form

$$\begin{aligned}
\dot{\hat{\boldsymbol{\varphi}}} &= \hat{\mathbf{v}} \\
\mathbf{M}_{\varphi}^{\rho}\dot{\hat{\mathbf{v}}} &= -\boldsymbol{\Phi}(\hat{\boldsymbol{\varphi}})\mathbf{M}_{\mathbf{C}}^{-1}\partial_{\hat{\mathbf{C}}}U - \boldsymbol{\Psi}(\hat{\boldsymbol{\varphi}})\mathbf{M}_{\mathbf{C}}^{-1}\partial_{\hat{\mathbf{G}}}U - \boldsymbol{\Xi}(\hat{\boldsymbol{\varphi}})\mathbf{M}_{J}^{-1}\partial_{J}U + \mathbf{g} + \mathbf{b} + \mathbf{t} \\
\mathbf{M}_{\mathbf{C}}\left\{\dot{\hat{\mathbf{C}}}\right\}_{\mathrm{V}} &= \boldsymbol{\Phi}^{\mathrm{T}}(\hat{\boldsymbol{\varphi}})\hat{\mathbf{v}} \\
\mathbf{M}_{\mathbf{C}}\left\{\dot{\hat{\mathbf{G}}}\right\}_{\mathrm{V}} &= \boldsymbol{\Psi}^{\mathrm{T}}(\hat{\boldsymbol{\varphi}})\hat{\mathbf{v}} \\
\mathbf{M}_{J}\dot{\hat{\mathbf{J}}} &= \boldsymbol{\Xi}^{\mathrm{T}}(\hat{\boldsymbol{\varphi}})\hat{\mathbf{v}}\,.
\end{aligned} \tag{85}$$

Note that on element level, $\left\{\dot{\hat{\mathbf{C}}}\right\}_{\mathrm{V}}$, $\left\{\dot{\hat{\mathbf{G}}}\right\}_{\mathrm{V}}$ and $\dot{\hat{\mathbf{J}}}$ can be expressed in terms of the nodal quantities $\hat{\boldsymbol{\varphi}}$ and $\hat{\mathbf{v}}$ by using the last three equations of (85). This implies that after the temporal discretization, the degrees of freedom corresponding to the strain-type fields $\mathbf{C}^{\mathrm{h}}$, $\mathbf{G}^{\mathrm{h}}$ and J^{h} can be eliminated by static condensation on element level (see Section 5.1.2). However, before proceeding with the

time discretization, we first show that (85) gives rise to a discrete pH system. For that purpose, we rewrite (85) in the form

$$\begin{bmatrix} \mathbf{I} & 0 & 0 & 0 & 0 \\ 0 & \mathbf{M}_{\varphi}^{\rho} & 0 & 0 & 0 \\ 0 & 0 & \mathbf{M}_{\mathbf{C}} & 0 & 0 \\ 0 & 0 & 0 & \mathbf{M}_{\mathbf{C}} & 0 \\ 0 & 0 & 0 & 0 & \mathbf{M}_{\mathbf{J}} \end{bmatrix} \begin{bmatrix} \dot{\hat{\boldsymbol{\varphi}}} \\ \dot{\hat{\mathbf{v}}} \\ \{\dot{\hat{\mathbf{C}}}\}_{\mathrm{V}} \\ \{\dot{\hat{\mathbf{G}}}\}_{\mathrm{V}} \\ \dot{\hat{\mathbf{J}}} \end{bmatrix} = \begin{bmatrix} 0 & \mathbf{I} & 0 & 0 & 0 \\ -\mathbf{I} & 0 & -\boldsymbol{\Phi}(\hat{\boldsymbol{\varphi}}) & -\boldsymbol{\Psi}(\hat{\boldsymbol{\varphi}}) & -\boldsymbol{\Xi}(\hat{\boldsymbol{\varphi}}) \\ 0 & \boldsymbol{\Phi}^{\mathrm{T}}(\hat{\boldsymbol{\varphi}}) & 0 & 0 & 0 \\ 0 & \boldsymbol{\Psi}^{\mathrm{T}}(\hat{\boldsymbol{\varphi}}) & 0 & 0 & 0 \\ 0 & \boldsymbol{\Xi}^{\mathrm{T}}(\hat{\boldsymbol{\varphi}}) & 0 & 0 & 0 \end{bmatrix} \begin{bmatrix} -\mathbf{g} \\ \hat{\mathbf{v}} \\ \mathbf{M}_{\mathbf{C}}^{-1}\partial_{\hat{\mathbf{C}}}U \\ \mathbf{M}_{\mathbf{C}}^{-1}\partial_{\hat{\mathbf{G}}}U \\ \mathbf{M}_{J}^{-1}\partial_{\hat{J}}U \end{bmatrix} + \begin{bmatrix} 0 & 0 \\ \mathbf{I} & \mathbf{I} \\ 0 & 0 \\ 0 & 0 \\ 0 & 0 \end{bmatrix} \begin{bmatrix} \mathbf{b} \\ \mathbf{t} \end{bmatrix} . \tag{86}$$

The above system of ordinary differential equations can be rewritten as

$$\mathbf{E}\dot{\hat{\mathbf{x}}} = \mathbf{J}(\hat{\boldsymbol{\varphi}})\mathbf{z}(\hat{\mathbf{x}}) + \mathbf{B}\hat{\mathbf{u}} \, , \tag{87}$$

where

$$\mathbf{E}^{\mathrm{T}}\mathbf{z}(\hat{\mathbf{x}}) = \nabla H(\hat{\mathbf{x}}) \, . \tag{88}$$

Similarly to the continuous version of the pH system in (20) and (21), the two equations (87) and (88) constitute a discrete pH system [31,32]. It can be easily observed that the structure matrix $\mathbf{J}$ is skew-symmetric. Moreover, the discrete Hamiltonian $H(\hat{\mathbf{x}})$ follows from the Hamiltonian (17) by inserting the space-discrete approximations dealt with previously. Consequently,

$$H(\hat{\mathbf{x}}) := \mathcal{H}^{\mathrm{h}} = \int_{\Omega_0} \big(\tfrac{1}{2}\rho_0 \mathbf{v}^{\mathrm{h}} \cdot \mathbf{v}^{\mathrm{h}} + \widetilde{\mathcal{W}}(\mathbf{C}^{\mathrm{h}}, \mathbf{G}^{\mathrm{h}}, J^{\mathrm{h}}) - \bar{\mathbf{g}} \cdot \boldsymbol{\varphi}^{\mathrm{h}}\big) \, \mathrm{dV} = \frac{1}{2}\hat{\mathbf{v}}^{\mathrm{T}}\mathbf{M}_{\varphi}^{\rho}\hat{\mathbf{v}} + \mathrm{U}\big(\{\hat{\mathbf{C}}\}_{\mathrm{V}}, \{\hat{\mathbf{G}}\}_{\mathrm{V}}, \hat{\mathbf{J}}\big) - \hat{\boldsymbol{\varphi}}^{\mathrm{T}}\mathbf{g} \, , \tag{89}$$

where the discrete stored energy U has been introduced in (76). Now, the derivative of the discrete Hamiltonian can be calculated to be

$$\nabla H(\hat{\mathbf{x}}) = \begin{bmatrix} -\mathbf{g} \\ \mathbf{M}_{\varphi}^{\rho}\hat{\mathbf{v}} \\ \partial_{\hat{\mathbf{C}}}U \\ \partial_{\hat{\mathbf{G}}}U \\ \partial_{\hat{J}}U \end{bmatrix} . \tag{90}$$

Note that the derivatives $\partial_{\hat{\mathbf{C}}}U$, $\partial_{\hat{\mathbf{G}}}U$ and $\partial_{\hat{J}}U$ have been defined in (78). The validity of (88) can now be easily verified.

Remark 2. The discrete pH system on the element level gives rise to a corresponding discrete pH system on the system level, since (i) the power-preserving interconnection of discrete pH systems yields again a discrete pH system, and (ii) the finite element assembly procedure can be viewed as power-preserving interconnection of the element contributions.

Remark 3. The pH form of the semi-discrete equations of motion guarantees the energy consistency of the space-discrete formulation. To see this, consider

$$\frac{\mathrm{d}}{\mathrm{d}t}H(\hat{\mathbf{x}}) = \nabla H(\hat{\mathbf{x}}) \cdot \dot{\hat{\mathbf{x}}} = \big(\mathbf{E}^{\mathrm{T}}\mathbf{z}(\hat{\mathbf{x}})\big) \cdot \dot{\hat{\mathbf{x}}} = \mathbf{z}(\hat{\mathbf{x}}) \cdot \mathbf{E}\dot{\hat{\mathbf{x}}} = \mathbf{z}(\hat{\mathbf{x}}) \cdot (\mathbf{J}(\hat{\boldsymbol{\varphi}})\mathbf{z}(\hat{\mathbf{x}}) + \mathbf{B}\hat{\mathbf{u}}) = \mathbf{z}(\hat{\mathbf{x}}) \cdot \mathbf{B}\hat{\mathbf{u}} = \hat{\mathbf{y}} \cdot \hat{\mathbf{u}} \tag{91}$$

where $\hat{\mathbf{y}} = \mathbf{B}^{\mathrm{T}}\mathbf{z}(\hat{\mathbf{x}})$ is the discrete output. Consequently, the total energy is conserved iff no external control forces $\hat{\mathbf{u}}$ act on the system.

Remark 4. In order for (87) and (88) to form a discrete pH system, the fulfillment of (88) is crucial. It should be noted that the presence of constitutive equations for the Lagrange multipliers in the weak form is required during the spatial discretization process to satisfy (88) in general. However, there is the following exception: The pointwise enforcement of the constitutive equations for the Lagrange multipliers is sufficient in the case of constant approximations for the strain-type mixed fields $\mathbf{C}$, $\mathbf{G}$ and J. In this case, $\mathbf{N}_C = \mathbf{I}_6$ and $\mathbf{N}_J = 1$, leading to $\mathbf{M}_{\mathbf{C}} = V_e\mathbf{I}_6$ and $\mathbf{M}_J = V_e$, where V_e is the volume of the element in the reference configuration.

5. Spatial and temporal discretization

In this section, the time-discrete weak form (53), introduced in Section 3, is further discretized in space. Although we shall deal with alternative spatial discretizations, we always start from the time-discrete weak form (53) corresponding to the fully mixed formulation.

5.1. Fully mixed element based on the strain-type fields $\{\mathbf{C}, \mathbf{G}, J\}$

In a first step, we apply the fully mixed finite element formulation devised in Section 4. Consequently, the time-discrete weak form (53) gives rise to

$$
\begin{aligned}
&\int_{\Omega_0} \mathbf{w}^{\mathrm{h}}_{\pi} \cdot \big(\frac{\boldsymbol{\varphi}^{\mathrm{h}}_{n+1} - \boldsymbol{\varphi}^{\mathrm{h}}_{n}}{\Delta t_n} - \mathbf{v}^{\mathrm{h}}_{n+1/2} \big) \,\mathrm{dV} = 0 \\
&\int_{\Omega_0} \mathbf{w}^{\mathrm{h}}_{\varphi} \cdot \rho_0 \frac{\mathbf{v}^{\mathrm{h}}_{n+1} - \mathbf{v}^{\mathrm{h}}_{n}}{\Delta t_n} + 2\,\mathrm{sym}(\mathbf{F}^{\mathrm{T}}_{\varphi^{\mathrm{h}}_{n+1/2}} \nabla \mathbf{w}^{\mathrm{h}}_{\varphi}) : \big(\boldsymbol{\Lambda}^{\mathrm{h}}_{\mathbf{C}_{n+1}} + \boldsymbol{\Lambda}^{\mathrm{h}}_{\mathbf{G}_{n+1}} \gg \mathbf{C}_{\varphi^{\mathrm{h}}_{n+1/2}} + \frac{\lambda^{\mathrm{h}}}{2 J_{\varphi^{\mathrm{h}}_{n+1/2}}} \mathbf{G}_{\varphi^{\mathrm{h}}_{n+1/2}} \big) \,\mathrm{dV} \\
&\quad = \int_{\Omega_0} \mathbf{w}^{\mathrm{h}}_{\varphi} \cdot \big(\bar{\mathbf{g}}_{n+1/2} + \bar{\mathbf{b}}_{n+1/2} \big) \,\mathrm{dV} + \int_{\partial\Omega_0} \mathbf{w}^{\mathrm{h}}_{\varphi} \cdot \bar{\mathbf{t}}_{n+1/2} \,\mathrm{dA} \\
&\int_{\Omega_0} \mathbf{w}^{\mathrm{h}}_{\mathbf{C}} : \big[\boldsymbol{\Lambda}^{\mathrm{h}}_{\mathbf{C}_{n+1}} - \mathrm{D}_{\mathbf{C}} \widetilde{\mathcal{W}}^{\mathrm{h}} \big] \,\mathrm{dV} = 0 \\
&\int_{\Omega_0} \mathbf{w}^{\mathrm{h}}_{\mathbf{G}} : \big[\boldsymbol{\Lambda}^{\mathrm{h}}_{\mathbf{G}_{n+1}} - \mathrm{D}_{\mathbf{G}} \widetilde{\mathcal{W}}^{\mathrm{h}} \big] \,\mathrm{dV} = 0 \\
&\int_{\Omega_0} w^{\mathrm{h}}_{J} \big[\lambda^{\mathrm{h}}_{n+1} - \mathrm{D}_{J} \widetilde{\mathcal{W}}^{\mathrm{h}} \big] \,\mathrm{dV} = 0 \\
&\int_{\Omega_0} \mathbf{w}^{\mathrm{h}}_{\boldsymbol{\Lambda}_{\mathbf{C}}} : \big[\frac{\mathbf{C}^{\mathrm{h}}_{n+1} - \mathbf{C}^{\mathrm{h}}_{n}}{\Delta t_n} - 2\,\mathrm{sym}(\mathbf{F}^{\mathrm{T}}_{\varphi^{\mathrm{h}}_{n+1/2}} \nabla \mathbf{v}^{\mathrm{h}}_{n+1/2}) \big] \,\mathrm{dV} = 0 \\
&\int_{\Omega_0} \mathbf{w}^{\mathrm{h}}_{\boldsymbol{\Lambda}_{\mathbf{G}}} : \big[\frac{\mathbf{G}^{\mathrm{h}}_{n+1} - \mathbf{G}^{\mathrm{h}}_{n}}{\Delta t_n} - 2\mathbf{C}_{\varphi^{\mathrm{h}}_{n+1/2}} \gg \mathrm{sym}(\mathbf{F}^{\mathrm{T}}_{\varphi^{\mathrm{h}}_{n+1/2}} \nabla \mathbf{v}^{\mathrm{h}}_{n+1/2}) \big] \,\mathrm{dV} = 0 \\
&\int_{\Omega_0} w^{\mathrm{h}}_{\lambda} \big[\frac{J^{\mathrm{h}}_{n+1} - J^{\mathrm{h}}_{n}}{\Delta t_n} - (J_{\varphi^{\mathrm{h}}_{n+1/2}})^{-1} \mathbf{G}_{\varphi^{\mathrm{h}}_{n+1/2}} : \mathrm{sym}(\mathbf{F}^{\mathrm{T}}_{\varphi^{\mathrm{h}}_{n+1/2}} \nabla \mathbf{v}^{\mathrm{h}}_{n+1/2}) \big] \,\mathrm{dV} = 0 \,.
\end{aligned}
\tag{92}
$$

Note that the discrete derivatives $\mathrm{D}_{\mathcal{V}^i} \widetilde{\mathcal{W}}(\mathcal{V}_n, \mathcal{V}_{n+1})$, $\mathcal{V}^i \in \{\mathbf{C}^{\mathrm{h}}, \mathbf{G}^{\mathrm{h}}, J^{\mathrm{h}}\}$, have been introduced in Section 3.

5.1.1. Fully mixed discrete port-Hamiltonian formulation

Since time and space discretization of the fully mixed formulation commutes, the scheme emanating from (92) can also be written in the form

$$
\mathbf{E}\big(\hat{\mathbf{x}}_{n+1} - \hat{\mathbf{x}}_n\big) = \Delta t_n \big(\mathbf{J}(\hat{\boldsymbol{\varphi}}_{n+1/2}) \bar{\mathbf{z}}(\hat{\mathbf{x}}_n, \hat{\mathbf{x}}_{n+1}) + \mathbf{B}\hat{\mathbf{u}}_{n+1/2} \big) \,,
\tag{93}
$$

where

$$
\mathbf{E}^{\mathrm{T}} \bar{\mathbf{z}}(\hat{\mathbf{x}}_n, \hat{\mathbf{x}}_{n+1}) = \bar{\nabla} H(\hat{\mathbf{x}}_n, \hat{\mathbf{x}}_{n+1}) \,.
\tag{94}
$$

Here, the matrices $\mathbf{E}$, $\mathbf{J}(\hat{\boldsymbol{\varphi}})$, and $\mathbf{B}$ can be again inferred from the discrete pH system (86). Moreover, the discrete derivative of the discrete Hamiltonian (89) is given by

$$
\bar{\nabla} H(\hat{\mathbf{x}}_n, \hat{\mathbf{x}}_{n+1}) = \begin{bmatrix} -\mathbf{g}_{n+1/2} \\ \mathbf{M}^{\rho}_{\varphi} \hat{\mathbf{v}}_{n+1/2} \\ \mathrm{D}_{\hat{\mathbf{C}}} U \\ \mathrm{D}_{\hat{\mathbf{G}}} U \\ \mathrm{D}_{\hat{J}} U \end{bmatrix},
\tag{95}
$$

where, similar to (78), the partitioned discrete derivatives of the discrete stored energy function assume the form

$$
\begin{aligned}
\mathrm{D}_{\hat{\mathbf{C}}} U &= \int_{\Omega_0} \mathbf{N}^{\mathrm{T}}_{C} \Big\{ \mathrm{D}_{\mathbf{C}} \widetilde{\mathcal{W}}^{\mathrm{h}} \Big\}_{\mathrm{V}} \mathrm{dV} \,, \\
\mathrm{D}_{\hat{\mathbf{G}}} U &= \int_{\Omega_0} \mathbf{N}^{\mathrm{T}}_{C} \Big\{ \mathrm{D}_{\mathbf{G}} \widetilde{\mathcal{W}}^{\mathrm{h}} \Big\}_{\mathrm{V}} \mathrm{dV} \,, \\
\mathrm{D}_{\hat{J}} U &= \int_{\Omega_0} \mathbf{N}_{J} \mathrm{D}_{J} \widetilde{\mathcal{W}}^{\mathrm{h}} \mathrm{dV} \,.
\end{aligned}
\tag{96}
$$

It should be noted that algorithmic conservation of the total energy and total angular momentum can be shown starting from (92) along the lines of Sections 3.1 and 3.2, respectively. Alternatively, the algorithmic conservation of energy can be verified using (93)

and (94). Consequently, due to the directionality property of the discrete derivative, we obtain

$$\begin{aligned} H(\hat{\mathbf{x}}_{n+1}) - H(\hat{\mathbf{x}}_n) &= \bar{\nabla} H(\hat{\mathbf{x}}_n, \hat{\mathbf{x}}_{n+1}) \cdot \left(\hat{\mathbf{x}}_{n+1} - \hat{\mathbf{x}}_n\right) \\ &= \left(\hat{\mathbf{x}}_{n+1} - \hat{\mathbf{x}}_n\right) \cdot \mathbf{E}^{\mathrm{T}} \bar{\mathbf{z}}(\hat{\mathbf{x}}_n, \hat{\mathbf{x}}_{n+1}) \\ &= \bar{\mathbf{z}}(\hat{\mathbf{x}}_n, \hat{\mathbf{x}}_{n+1}) \cdot \mathbf{E}\left(\hat{\mathbf{x}}_{n+1} - \hat{\mathbf{x}}_n\right) \\ &= \Delta t_n \bar{\mathbf{z}}(\hat{\mathbf{x}}_n, \hat{\mathbf{x}}_{n+1}) \cdot \left(\mathbf{J}(\hat{\boldsymbol{\varphi}}_{n+1/2}) \bar{\mathbf{z}}(\hat{\mathbf{x}}_n, \hat{\mathbf{x}}_{n+1}) + \mathbf{B}\hat{\mathbf{u}}_{n+1/2}\right) \\ &= \Delta t_n \left(\mathbf{B}^{\mathrm{T}} \bar{\mathbf{z}}(\hat{\mathbf{x}}_n, \hat{\mathbf{x}}_{n+1})\right) \cdot \hat{\mathbf{u}}_{n+1/2} \\ &= \Delta t_n \hat{\mathbf{y}}_{n+1/2} \cdot \hat{\mathbf{u}}_{n+1/2} \,, \end{aligned} \tag{97}$$

where $\hat{\mathbf{y}}_{n+1/2} = \mathbf{B}^{\mathrm{T}} \bar{\mathbf{z}}(\hat{\mathbf{x}}_n, \hat{\mathbf{x}}_{n+1})$ is the discrete output at time $t_{n+1/2}$.

5.1.2. Notes on the implementation

An efficient implementation of the fully mixed formulation can be reached by applying static condensation of the mixed strain-type variables and expressing the nodal velocities $\hat{\mathbf{v}}_{n+1}$ in terms of the nodal position vectors $\hat{\boldsymbol{\varphi}}_{n+1}$. At the element level, the fully discrete equations (93) and (94) can be written in the form

$$\begin{aligned} \hat{\boldsymbol{\varphi}}_{n+1} - \hat{\boldsymbol{\varphi}}_n &= \Delta t_n \hat{\mathbf{v}}_{n+1/2} \\ \frac{1}{\Delta t_n} \mathbf{M}_\varphi^\rho \left(\hat{\mathbf{v}}_{n+1} - \hat{\mathbf{v}}_n\right) &= -\boldsymbol{\Phi}(\hat{\boldsymbol{\varphi}}_{n+1/2}) \mathbf{M}_{\mathbf{C}}^{-1} \mathrm{D}_{\hat{\mathbf{C}}} U - \boldsymbol{\Psi}(\hat{\boldsymbol{\varphi}}_{n+1/2}) \mathbf{M}_{\mathbf{C}}^{-1} \mathrm{D}_{\hat{\mathbf{G}}} U - \boldsymbol{\Xi}(\hat{\boldsymbol{\varphi}}_{n+1/2}) \mathbf{M}_J^{-1} \mathrm{D}_{\hat{J}} U + \mathbf{g}_{n+1/2} + \mathbf{b}_{n+1/2} + \mathbf{t}_{n+1/2} \\ \frac{1}{\Delta t_n} \mathbf{M}_{\mathbf{C}} \left(\left\{ \hat{\mathbf{C}}_{n+1} \right\}_{\mathrm{V}} - \left\{ \hat{\mathbf{C}}_n \right\}_{\mathrm{V}} \right) &= \boldsymbol{\Phi}^{\mathrm{T}}(\hat{\boldsymbol{\varphi}}_{n+1/2}) \hat{\mathbf{v}}_{n+1/2} \\ \frac{1}{\Delta t_n} \mathbf{M}_{\mathbf{C}} \left(\left\{ \hat{\mathbf{G}}_{n+1} \right\}_{\mathrm{V}} - \left\{ \hat{\mathbf{G}}_n \right\}_{\mathrm{V}} \right) &= \boldsymbol{\Psi}^{\mathrm{T}}(\hat{\boldsymbol{\varphi}}_{n+1/2}) \hat{\mathbf{v}}_{n+1/2} \\ \frac{1}{\Delta t_n} \mathbf{M}_J \left(\hat{\mathbf{J}}_{n+1} - \hat{\mathbf{J}}_n \right) &= \boldsymbol{\Xi}^{\mathrm{T}}(\hat{\boldsymbol{\varphi}}_{n+1/2}) \hat{\mathbf{v}}_{n+1/2} \end{aligned} \tag{98}$$

(cf. (85)). We now introduce the element residual vector

$$\begin{aligned} \mathbf{R}(\hat{\boldsymbol{\varphi}}_{n+1}) := \frac{2}{\Delta t_n} \mathbf{M}_\varphi^\rho \left(\hat{\boldsymbol{\varphi}}_{n+1} - \hat{\boldsymbol{\varphi}}_n\right) - 2\mathbf{M}_\varphi^\rho \hat{\mathbf{v}}_n + \Delta t_n \boldsymbol{\Phi}(\hat{\boldsymbol{\varphi}}_{n+1/2}) \mathbf{M}_{\mathbf{C}}^{-1} \mathrm{D}_{\hat{\mathbf{C}}} U \\ + \Delta t_n \left(\boldsymbol{\Psi}(\hat{\boldsymbol{\varphi}}_{n+1/2}) \mathbf{M}_{\mathbf{C}}^{-1} \mathrm{D}_{\hat{\mathbf{G}}} U + \boldsymbol{\Xi}(\hat{\boldsymbol{\varphi}}_{n+1/2}) \mathbf{M}_J^{-1} \mathrm{D}_{\hat{J}} U - \mathbf{g}_{n+1/2} - \mathbf{b}_{n+1/2} - \mathbf{t}_{n+1/2} \right) \,, \end{aligned} \tag{99}$$

where the discrete derivatives of the discrete stored energy, $\mathrm{D}_{\hat{\mathbf{C}}} U$, $\mathrm{D}_{\hat{\mathbf{G}}} U$ and $\mathrm{D}_{\hat{J}} U$, are defined in (96). Thus, to calculate the residual vector (99), one first has to calculate

$$\begin{aligned} \left\{ \hat{\mathbf{C}}_{n+1} \right\}_{\mathrm{V}} &= \left\{ \hat{\mathbf{C}}_n \right\}_{\mathrm{V}} + \Delta t_n \mathbf{M}_{\mathbf{C}}^{-1} \boldsymbol{\Phi}^{\mathrm{T}}(\hat{\boldsymbol{\varphi}}_{n+1/2}) \hat{\mathbf{v}}_{n+1/2} \\ \left\{ \hat{\mathbf{G}}_{n+1} \right\}_{\mathrm{V}} &= \left\{ \hat{\mathbf{G}}_n \right\}_{\mathrm{V}} + \Delta t_n \mathbf{M}_{\mathbf{C}}^{-1} \boldsymbol{\Psi}^{\mathrm{T}}(\hat{\boldsymbol{\varphi}}_{n+1/2}) \hat{\mathbf{v}}_{n+1/2} \\ \hat{\mathbf{J}}_{n+1} &= \hat{\mathbf{J}}_n + \Delta t_n \mathbf{M}_J^{-1} \boldsymbol{\Xi}^{\mathrm{T}}(\hat{\boldsymbol{\varphi}}_{n+1/2}) \hat{\mathbf{v}}_{n+1/2} \,. \end{aligned} \tag{100}$$

These equations result from the last three equations in (98). In this context, $\hat{\mathbf{v}}_{n+1/2} = {}^{(\hat{\boldsymbol{\varphi}}_{n+1} - \hat{\boldsymbol{\varphi}}_n)}/_{\Delta t_n}$ results from the first equation in (98). Now,

$$\begin{aligned} \left\{ \mathbf{C}_{n+1}^{\mathrm{h}} \right\}_{\mathrm{V}} &= \mathbf{M} \left\{ \hat{\mathbf{C}}_{n+1} \right\}_{\mathrm{V}} \,, \\ \left\{ \mathbf{G}_{n+1}^{\mathrm{h}} \right\}_{\mathrm{V}} &= \mathbf{M} \left\{ \hat{\mathbf{G}}_{n+1} \right\}_{\mathrm{V}} \,, \\ J_{n+1}^{\mathrm{h}} &= \bar{\mathbf{M}} \hat{\mathbf{J}}_{n+1} \end{aligned} \tag{101}$$

can be used to evaluate the discrete derivatives (56) required to determine $\mathrm{D}_{\hat{\mathbf{C}}} U$, $\mathrm{D}_{\hat{\mathbf{G}}} U$ and $\mathrm{D}_{\hat{J}} U$ through (96).

The residual vector of the whole system can be obtained from the assembly of the element contributions (99) by applying standard finite element procedures. It should be noted that static condensation of mixed strain-type unknowns at element level leads to history-type quantities $\left\{ \hat{\mathbf{C}}_n \right\}_{\mathrm{V}}$, $\left\{ \hat{\mathbf{G}}_n \right\}_{\mathrm{V}}$ and $\hat{\mathbf{J}}_n$ in (100), which must be recovered from storage in each time step. We eventually emphasize that after finite element assembly, merely the nodal position vectors at time t_{n+1} remain as unknowns of the resulting nonlinear algebraic system, which can be solved iteratively by applying Newton's method. Consequently, the numerical effort to solve the global algebraic system is comparable to that of the purely displacement-based formulation treated in Section 5.3.

5.2. Mixed element based on the strain-type fields $\{\mathbf{G}, J\}$

We next show that the time-discrete weak form (53) can also accommodate the mixed finite element formulation developed in [25,26], which is based on independent finite element approximations of mixed fields $\mathbf{G}$ and J. The corresponding size reduction of the time-discrete weak form (53) is based on the following two steps:

1. Choose the test function $\mathbf{w}_{\mathbf{C}}$ in (53) to be of the form

$$\mathbf{w}_{\mathbf{C}} = -2\,\mathrm{sym}(\mathbf{F}^{\mathrm{T}}_{\boldsymbol{\varphi}_{n+1/2}} \nabla \mathbf{w}_{\varphi}) \tag{102}$$

for arbitrary $\mathbf{w}_{\varphi} \in \mathcal{V}^0_{\varphi}$.

2. Due to the arbitrariness of $\mathbf{w}_{\boldsymbol{\Lambda}_{\mathbf{C}}} \in \mathcal{V}_C$, the update formula for $\mathbf{C}_{n+1}$ in (53) can be evaluated at Gauss point level, leading to

$$\mathbf{C}_{n+1} = \mathbf{C}_n + \Delta t_n 2\,\mathrm{sym}(\mathbf{F}^{\mathrm{T}}_{\boldsymbol{\varphi}_{n+1/2}} \nabla \mathbf{v}_{n+1/2})\,. \tag{103}$$

Provided that $\mathbf{C}_n = \mathbf{C}_{\varphi^{\mathrm{h}}_n}$, a straightforward calculation based on (103) shows that $\mathbf{C}_{n+1} = \mathbf{C}_{\varphi^{\mathrm{h}}_{n+1}}$. For completeness, this is shown in Appendix A.3.

The remaining equations of the time-discrete weak form (53) can now be used to accommodate the mixed finite element formulation due to [25,26]. The resulting scheme emanates from

$$\begin{aligned}
&\int_{\Omega_0} \mathbf{w}^{\mathrm{h}}_{\pi} \cdot \Big(\frac{\boldsymbol{\varphi}^{\mathrm{h}}_{n+1} - \boldsymbol{\varphi}^{\mathrm{h}}_{n}}{\Delta t_n} - \mathbf{v}^{\mathrm{h}}_{n+1/2} \Big)\,\mathrm{dV} = 0 \\
&\int_{\Omega_0} \mathbf{w}^{\mathrm{h}}_{\varphi} \cdot \rho_0 \frac{\mathbf{v}^{\mathrm{h}}_{n+1} - \mathbf{v}^{\mathrm{h}}_{n}}{\Delta t_n} + 2\,\mathrm{sym}(\mathbf{F}^{\mathrm{T}}_{\varphi^{\mathrm{h}}_{n+1/2}} \nabla \mathbf{w}^{\mathrm{h}}_{\varphi}) : \Big(\mathrm{D}_{\mathbf{C}} \widetilde{\mathcal{W}}^{\mathrm{h}} + \boldsymbol{\Lambda}^{\mathrm{h}}_{\mathbf{G}_{n+1}} \mathbin{\ggg} \mathbf{C}_{\varphi^{\mathrm{h}}_{n+1/2}} + \frac{\lambda^{\mathrm{h}}_{n+1}}{2 J_{\varphi^{\mathrm{h}}_{n+1/2}}} \mathbf{G}_{\varphi^{\mathrm{h}}_{n+1/2}} \Big)\,\mathrm{dV} \\
&\quad = \int_{\Omega_0} \mathbf{w}^{\mathrm{h}}_{\varphi} \cdot \big(\bar{\mathbf{g}}_{n+1/2} + \bar{\mathbf{b}}_{n+1/2} \big)\,\mathrm{dV} + \int_{\partial\Omega_0} \mathbf{w}^{\mathrm{h}}_{\varphi} \cdot \bar{\mathbf{t}}_{n+1/2}\,\mathrm{dA} \\
&\int_{\Omega_0} \mathbf{w}^{\mathrm{h}}_{\mathbf{G}} : \Big[\boldsymbol{\Lambda}^{\mathrm{h}}_{\mathbf{G}_{n+1}} - \mathrm{D}_{\mathbf{G}} \widetilde{\mathcal{W}}^{\mathrm{h}} \Big]\,\mathrm{dV} = 0 \\
&\int_{\Omega_0} w^{\mathrm{h}}_{J} \Big[\lambda^{\mathrm{h}}_{n+1} - \mathrm{D}_{J} \widetilde{\mathcal{W}}^{\mathrm{h}} \Big]\,\mathrm{dV} = 0 \\
&\int_{\Omega_0} \mathbf{w}^{\mathrm{h}}_{\boldsymbol{\Lambda}_{\mathbf{G}}} : \Big[\frac{\mathbf{G}^{\mathrm{h}}_{n+1} - \mathbf{G}^{\mathrm{h}}_{n}}{\Delta t_n} - 2\mathbf{C}_{\varphi^{\mathrm{h}}_{n+1/2}} \mathbin{\ggg} \mathrm{sym}(\mathbf{F}^{\mathrm{T}}_{\varphi^{\mathrm{h}}_{n+1/2}} \nabla \mathbf{v}^{\mathrm{h}}_{n+1/2}) \Big]\,\mathrm{dV} = 0 \\
&\int_{\Omega_0} w^{\mathrm{h}}_{\lambda} \Big[\frac{J^{\mathrm{h}}_{n+1} - J^{\mathrm{h}}_{n}}{\Delta t_n} - (J_{\varphi^{\mathrm{h}}_{n+1/2}})^{-1} \mathbf{G}_{\varphi^{\mathrm{h}}_{n+1/2}} : \mathrm{sym}(\mathbf{F}^{\mathrm{T}}_{\varphi^{\mathrm{h}}_{n+1/2}} \nabla \mathbf{v}^{\mathrm{h}}_{n+1/2}) \Big]\,\mathrm{dV} = 0
\end{aligned} \tag{104}$$

with

$$\mathbf{C}_{n+1} = \mathbf{C}_{\varphi^{\mathrm{h}}_{n+1}} \quad \text{and} \quad \mathbf{C}_n = \mathbf{C}_{\varphi^{\mathrm{h}}_{n}}\,. \tag{105}$$

The finite element approximation of the remaining fields in (104) can be done in complete analogy to the fully mixed formulation as described in Section 4.1.

Algorithmic conservation of the total energy and total angular momentum can be shown by following similar lines as in Sections 3.1 and 3.2, respectively.

The implementation of the resulting EM scheme again relies on static condensation of the remaining mixed fields and can be performed in complete analogy to the fully mixed formulation (see Section 5.1.2).

5.3. Displacement-based element

We next show that the time-discrete weak form (53) can also accommodate purely displacement-based elements. The corresponding size reduction of the time-discrete weak form (53) is based on the following two steps:

1. Choose the test functions $\mathbf{w}_{\mathbf{C}}$, $\mathbf{w}_{\mathbf{G}}$ and w_J in (53) to be of the form

$$\begin{aligned}
\mathbf{w}_{\mathbf{C}} &= -2\,\mathrm{sym}(\mathbf{F}^{\mathrm{T}}_{\boldsymbol{\varphi}_{n+1/2}} \nabla \mathbf{w}_{\varphi}) \\
\mathbf{w}_{\mathbf{G}} &= -2\,\mathrm{sym}(\mathbf{F}^{\mathrm{T}}_{\boldsymbol{\varphi}_{n+1/2}} \nabla \mathbf{w}_{\varphi}) \mathbin{\ggg} \mathbf{C}_{\boldsymbol{\varphi}_{n+1/2}} \\
w_J &= -\boldsymbol{J}^{-1}_{\boldsymbol{\varphi}_{n+1/2}}\, \mathrm{sym}(\mathbf{F}^{\mathrm{T}}_{\boldsymbol{\varphi}_{n+1/2}} \nabla \mathbf{w}_{\varphi}) : \mathbf{G}_{\boldsymbol{\varphi}_{n+1/2}}
\end{aligned} \tag{106}$$

for arbitrary $\mathbf{w}_{\varphi} \in \mathcal{V}^0_{\varphi}$.

2. Due to the arbitrariness of $\mathbf{w}_{\boldsymbol{\Lambda}_{\mathbf{C}}}, \mathbf{w}_{\boldsymbol{\Lambda}_{\mathbf{G}}} \in \mathcal{V}_C$ and $w_{\lambda} \in \mathcal{V}_J$, the update formulas for $\mathbf{C}_{n+1}$, $\mathbf{G}_{n+1}$ and J_{n+1} in (53) can be evaluated at Gauss point level leading to

$$\begin{aligned}
\mathbf{C}_{n+1} &= \mathbf{C}_{\varphi^{\mathrm{h}}_{n+1}} \\
\mathbf{G}_{n+1} &= \mathbf{G}_n + 2\Delta t_n \mathbf{C}_{\varphi^{\mathrm{h}}_{n+1/2}} \mathbin{\ggg} \mathrm{sym}(\mathbf{F}^{\mathrm{T}}_{\varphi^{\mathrm{h}}_{n+1/2}} \nabla \mathbf{v}^{\mathrm{h}}_{n+1/2}) \\
J_{n+1} &= J_n + \frac{\Delta t_n}{J_{\varphi^{\mathrm{h}}_{n+1/2}}} \mathbf{G}_{\varphi^{\mathrm{h}}_{n+1/2}} : \mathrm{sym}(\mathbf{F}^{\mathrm{T}}_{\varphi^{\mathrm{h}}_{n+1/2}} \nabla \mathbf{v}^{\mathrm{h}}_{n+1/2})\,.
\end{aligned} \tag{107}$$

Here, $(107)_1$ again results from (103) as shown in Appendix A.3

Table 1
Considered discretizations and associated abbreviations.

FM-Q_2Q_1-EM	fully mixed formulation (see Section 5.1): spatially continuous triquadratic Q_2-elements for $\mathbf{v}$, $\boldsymbol{\varphi}$, and discontinuous trilinear Q_1-elements for $\mathbf{C}$, $\mathbf{G}$, J, $\boldsymbol{\Lambda}_{\mathbf{C}}$, $\boldsymbol{\Lambda}_{\mathbf{G}}$, λ; EM scheme
FM-Q_1Q_0-EM	fully mixed formulation (see Section 5.1): spatially continuous trilinear Q_1-elements for $\mathbf{v}$, $\boldsymbol{\varphi}$, and discontinuous constant Q_0-elements for $\mathbf{C}$, $\mathbf{G}$, J, $\boldsymbol{\Lambda}_{\mathbf{C}}$, $\boldsymbol{\Lambda}_{\mathbf{G}}$, λ; EM scheme
RM-Q_2Q_1-EM	size-reduced mixed formulation (see Section 5.2): spatially continuous triquadratic Q_2-elements for $\mathbf{v}$, $\boldsymbol{\varphi}$, and discontinuous trilinear Q_1-elements for $\mathbf{G}$, J, $\boldsymbol{\Lambda}_{\mathbf{G}}$, λ; EM scheme
RM-Q_1Q_0-EM	size-reduced mixed formulation (see Section 5.2): spatially continuous trilinear Q_1-elements for $\mathbf{v}$, $\boldsymbol{\varphi}$, and discontinuous constant Q_0-elements for $\mathbf{G}$, J, $\boldsymbol{\Lambda}_{\mathbf{G}}$, λ; EM scheme
RD-Q_1-EM	size-reduced displacement formulation (see Section 5.3): spatially continuous trilinear Q_1-elements for $\mathbf{v}$, $\boldsymbol{\varphi}$; EM scheme
SD-Q_1-MP	standard displacement-based formulation: spatially continuous trilinear Q_1-elements for $\mathbf{v}$, $\boldsymbol{\varphi}$; implicit midpoint rule
SD-Q_1-EM	standard displacement-based formulation: spatially continuous trilinear Q_1-elements for $\mathbf{v}$, $\boldsymbol{\varphi}$; EM scheme (see Remark 5)

Inserting the test functions from (106) into (53) gives rise to the following displacement-based formulation

$$\begin{aligned}
&\int_{\Omega_0} \mathbf{w}^{\mathrm{h}}_{\pi} \cdot \Big(\frac{\boldsymbol{\varphi}^{\mathrm{h}}_{n+1} - \boldsymbol{\varphi}^{\mathrm{h}}_{n}}{\Delta t_n} - \mathbf{v}^{\mathrm{h}}_{n+1/2} \Big) \,\mathrm{dV} = 0 \\
&\int_{\Omega_0} \mathbf{w}^{\mathrm{h}}_{\varphi} \cdot \rho_0 \frac{\mathbf{v}^{\mathrm{h}}_{n+1} - \mathbf{v}^{\mathrm{h}}_{n}}{\Delta t_n} + \mathrm{sym}(\mathbf{F}^{\mathrm{T}}_{\varphi^{\mathrm{h}}_{n+1/2}} \nabla \mathbf{w}^{\mathrm{h}}_{\varphi}) : \mathbf{S}_{\mathrm{A}} \,\mathrm{dV} = \int_{\Omega_0} \mathbf{w}^{\mathrm{h}}_{\varphi} \cdot \big(\bar{\mathbf{g}}_{\mathrm{n+1/2}} + \bar{\mathbf{b}}_{\mathrm{n+1/2}} \big) \,\mathrm{dV} + \int_{\partial\Omega_0} \mathbf{w}^{\mathrm{h}}_{\varphi} \cdot \bar{\mathbf{t}}_{\mathrm{n+1/2}} \,\mathrm{dA}
\end{aligned} \tag{108}$$

with algorithmic stress formula

$$\mathbf{S}_{\mathrm{A}} = 2\mathrm{D}_{\mathbf{C}} \widetilde{\mathcal{W}} + 2\mathrm{D}_{\mathbf{G}} \widetilde{\mathcal{W}} \gg \mathbf{C}_{\varphi^{\mathrm{h}}_{n+1/2}} + \frac{\mathrm{D}_J \widetilde{\mathcal{W}}}{J_{\varphi^{\mathrm{h}}_{n+1/2}}} \mathbf{G}_{\varphi^{\mathrm{h}}_{n+1/2}} \,, \tag{109}$$

in which strain-type quantities (107) are required to calculate the discrete derivatives $\mathrm{D}_{\mathcal{V}^i} \widetilde{\mathcal{W}}(\mathcal{V}_n, \mathcal{V}_{n+1})$, $\mathcal{V}^i \in \{\mathbf{C}, \mathbf{G}, J\}$, at the Gauss point level. Note that $\mathbf{G}_n$ and J_n play the role of history variables that must be retrieved from storage at each time step to calculate $\mathbf{G}_{n+1}$ and J_{n+1} from $(107)_{2,3}$. In contrast to that, $\mathbf{C}_{n+1}$ can be obtained directly from $\boldsymbol{\varphi}^{\mathrm{h}}_{n+1}$ by applying $(107)_1$.

Algorithmic conservation of the total energy can be shown following lines similar to those in Section 3.1. Consequently, choosing $\mathbf{w}^{\mathrm{h}}_{\varphi} = \mathbf{v}^{\mathrm{h}}_{n+1/2}$ and taking into account (107), a straightforward calculation shows the conservation of the total energy in the absence of external forces. Similarly to Section 3.2, conservation of angular momentum can be shown by choosing $\mathbf{w}^{\mathrm{h}}_{\varphi} = \boldsymbol{\zeta} \times \mathbf{v}^{\mathrm{h}}_{n+1/2}$.

Remark 5. The distinguishing features of the present approach to the formulation of EM schemes are (i) the partitioned form of the algorithmic stress formula (109) relying on partial discrete derivatives of the strain energy $\widetilde{\mathcal{W}}(\mathbf{C}, \mathbf{G}, J)$ (cf. Example 1) and (ii) the update formulas (107) for the strain-type variables relying on history variables $\mathbf{G}_n$ and J_n.
This is in contrast to previous developments [20,21] relying on discrete derivatives of the strain energy $\widehat{\mathcal{W}}(\mathbf{C}_{\varphi})$ defined in (9). In particular, applying the discrete derivative proposed in [20] yields an algorithmic stress formula of the form $\mathbf{S}_{\mathrm{A}} = 2\mathrm{D}_{\mathbf{C}} \widehat{\mathcal{W}}$, where

$$\mathrm{D}_{\mathbf{C}} \widehat{\mathcal{W}} = \nabla_{\mathbf{C}} \widehat{\mathcal{W}}(\mathbf{C}_{n+1/2}) + \frac{\widehat{\mathcal{W}}(\mathbf{C}_{n+1}) - \widehat{\mathcal{W}}(\mathbf{C}_n) - \nabla_{\mathbf{C}} \widehat{\mathcal{W}}(\mathbf{C}_{n+1/2}) : \Delta\mathbf{C}}{\Delta\mathbf{C} : \Delta\mathbf{C}} \Delta\mathbf{C} \,. \tag{110}$$

Here, $\mathbf{C}_n = \mathbf{C}_{\varphi^{\mathrm{h}}_n}$, $\mathbf{C}_{n+1} = \mathbf{C}_{\varphi^{\mathrm{h}}_{n+1}}$ and $\Delta\mathbf{C} = \mathbf{C}_{n+1} - \mathbf{C}_n$.

6. Numerical examples

This section presents numerical examples dealing with finite elastodynamics by applying various finite element formulations. In particular, we apply the newly developed EM schemes resulting from the fully mixed (FM) formulation (Section 5.1), the size-reduced mixed (RM) formulation (Section 5.2) and the size-reduced displacement (RD) formulation (Section 5.3). For comparison, we also apply the standard displacement-based (SD) formulation in combination with the implicit midpoint rule and the "projection-based" EM scheme (cf. [20] and Remark 5). The mixed formulations rely on globally continuous tri-linear or tri-quadratic interpolations for the displacements and velocities, while the mixed quantities are interpolated one order lower, discontinuously across the element boundaries allowing for a static condensation as described in Sections 4 and 5. The various formulations under investigation are summarized in Table 1.

Two hyperelastic material models are considered. A Mooney-Rivlin model (cf. [24]) with a stored energy function, defined as

$$\widetilde{\mathcal{W}}^{\mathrm{MR}} = a(\mathrm{tr}(\mathbf{C}) - 3) + b(\mathrm{tr}(\mathbf{G}) - 3) + \frac{c}{2}(J-1)^2 - d\ln(J) \,, \tag{111}$$

with independent parameters $a, b, c \in \mathbb{R}^+$ and dependent parameter $d = 2\,(a + 2\,b)$ that ensures stress normalization (stress-free reference configuration). For more details, refer to [36]. Furthermore, a modified Mooney-Rivlin model (cf. [25]), whose stored energy is given by

$$\widetilde{\mathcal{W}}^{\mathrm{mMR}} = \frac{\alpha}{2}\big((\mathrm{tr}(\mathbf{C}))^2 - 9\big) + \frac{\beta}{2}\big((\mathrm{tr}(\mathbf{G}))^2 - 9\big) - \gamma\ln(J) + \epsilon_1\big(J^{2\epsilon_2} + J^{-2\epsilon_2} - 2\big), \tag{112}$$

Table 2
Mooney-Rivlin model parameters from [36].

a	831.25	[Pa]
b	166.25	[Pa]
c	10000	[Pa]
$d = 2(a + 2b)$	2327.5	[Pa]
ρ_0	100	[kg m^{-3}]

Table 3
Modified Mooney-Rivlin model parameters from [25] with effective Poisson's ratio of $\nu = 0.495$.

α	42000	[Pa]
β	84000	[Pa]
$\gamma = 6(\alpha + 2\beta)$	1260000	[Pa]
ϵ_1	100000	[Pa]
ϵ_2	10	[-]
ρ_0	225	[kg m^{-3}]

Table 4
Modified Mooney-Rivlin model parameters inspired from [25] with effective Poisson's ratio of $\nu = 0.499$.

α	42000	[Pa]
β	84000	[Pa]
$\gamma = 6(\alpha + 2\beta)$	1260000	[Pa]
ϵ_1	150000	[Pa]
ϵ_2	17.7	[-]
ρ_0	225	[kg m^{-3}]

is considered, where the independent parameters $\alpha, \beta, \epsilon_1, \epsilon_2 \in \mathbb{R}^+$ are introduced and dependent parameter $\gamma = 6\,(\alpha + 2\,\beta)$ ensures stress normalization[2]

The specific model parameters for the numerical study of the first example (Section 6.1) are listed in Table 2 and result in a compressible material behavior. In contrast, the second example (Section 6.2) deals with quasi-incompressible material behavior. The parameters are listed in Tables 3 and 4. In both cases, a linearization of the employed material model about the reference configuration leads to a quasi-incompressible material behavior with an effective Poisson's ratios of $\nu = 0.495$ and $\nu = 0.499$, respectively.

The discrete derivatives of the stored energy functions required in the fully mixed formulation (Section 5.1), the size-reduced mixed formulation (Section 5.2), and the size-reduced displacement formulation (Section 5.3) can now be easily calculated. For the stored energy of the Mooney-Rivlin model (111) we obtain

$$\begin{aligned} \mathrm{D}_{\mathbf{C}}\widetilde{\mathcal{W}} &= a\mathbf{I}\,, \\ \mathrm{D}_{\mathbf{G}}\widetilde{\mathcal{W}} &= b\mathbf{I}\,, \\ \mathrm{D}_{J}\widetilde{\mathcal{W}} &= \frac{\frac{c}{2}(J_{n+1}-1)^2 - d\ln(J_{n+1}) - \left(\frac{c}{2}(J_n-1)^2 - d\ln(J_n)\right)}{J_{n+1}-J_n}\,. \end{aligned} \tag{113}$$

Similarly, the discrete derivatives of the modified Mooney-Rivlin model (112) are given by

$$\begin{aligned} \mathrm{D}_{\mathbf{C}}\widetilde{\mathcal{W}} &= \alpha\,\mathrm{tr}(\mathbf{C}_{n+1/2})\mathbf{I}\,, \\ \mathrm{D}_{\mathbf{G}}\widetilde{\mathcal{W}} &= \beta\,\mathrm{tr}(\mathbf{G}_{n+1/2})\mathbf{I}\,, \\ \mathrm{D}_{J}\widetilde{\mathcal{W}} &= \frac{-\gamma\left(\ln(J_{n+1}) - \ln(J_n)\right) + \epsilon_1\left(J_{n+1}^{2\epsilon_2} - J_n^{2\epsilon_2} + J_{n+1}^{-2\epsilon_2} - J_n^{-2\epsilon_2}\right)}{J_{n+1}-J_n}\,. \end{aligned} \tag{114}$$

Note that both stored energy functions under consideration are separable as outlined in Example 1.

6.1. Dynamical investigations of an L-shaped body

The objective of this first investigation is to assess the robustness, long-term stability, and discrete conservation properties of the newly developed formulations and integrators, compared to the standard midpoint integrator.

We consider the initial boundary value problem of an L-shaped body, following the work of [19,24,37].

[2] It should be emphasized that the above formulation differs from the one presented in [25] solely by an energy normalization (energy-free reference configuration), consistent with the standard Mooney-Rivlin model (111) (see also [36] for more details).

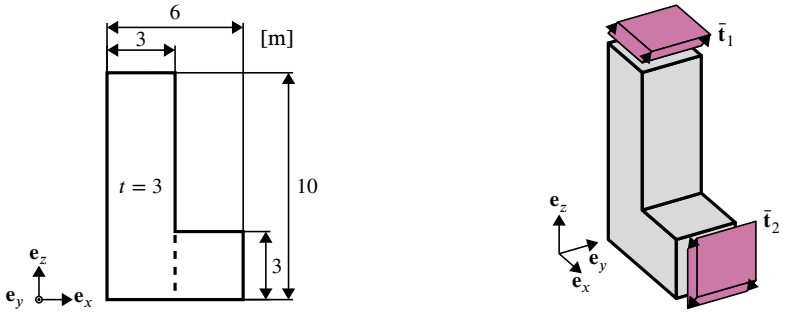

Fig. 2. 2D projection of the geometry (left) and 3D illustration of the boundary conditions (right) of the L-shaped body.

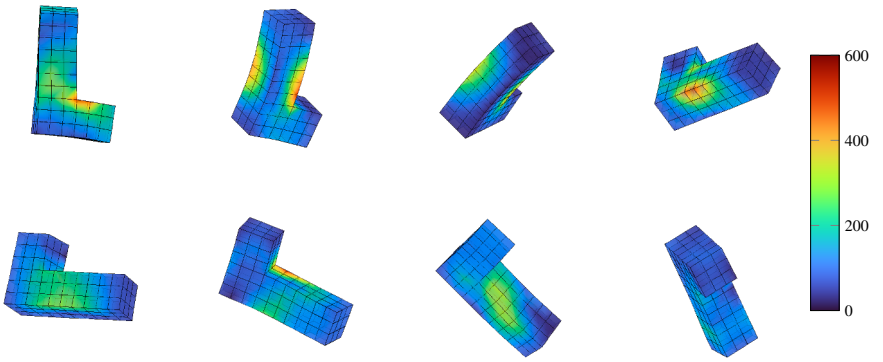

Fig. 3. Snapshots with von Mises stress distribution σ_{vM} [Pa] of the *FM*-Q_1Q_0-EM formulation at times $t \in \{3.0, 6.0, 9.0, 12.0, 15.0, 18.0, 21.0, 24.0\}$s.

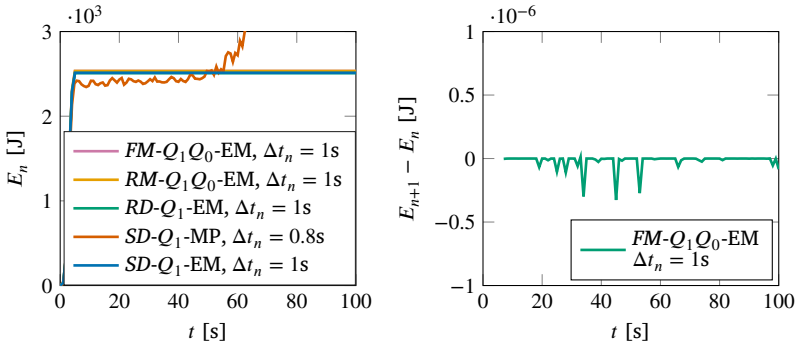

Fig. 4. Total energy of the L-shaped body (left) for the different formulations and integrators. The corresponding energy difference plot for the *FM*-Q_1Q_0-EM formulation is shown on the right, obtained with a Newton tolerance of $\epsilon = 1e\text{-}6$.

The geometry and initial setting with boundary conditions are shown in Fig. 2. In particular, the applied external tractions are

$$\bar{\mathbf{t}}_1(t) = -\bar{\mathbf{t}}_2(t) = f(t)\,\frac{1}{9}\begin{bmatrix}256\\512\\768\end{bmatrix}\frac{\text{N}}{\text{m}^2}, \qquad f(t) = \begin{cases} t & \text{for } t \le 2.5\text{s} \\ 5 - t & \text{for } 2.5\text{s} < t \le 5\text{s} \\ 0 & \text{for } t > 5\text{s}. \end{cases}$$

The L-shaped domain is discretized with 117 finite elements, and the simulation time is set to $T = 100\,\text{s}$. In Fig. 3, snapshots of the motion are shown with the corresponding von Mises stress distribution, clearly showing the occurrence of large rotations, deformations, and stresses.

The energies obtained with the integrators under investigation are shown in Fig. 4. Note that after $t = 5\text{s}$, no external forces are acting on the system, so that the total energy should be a constant of motion.

The total angular momentum obtained with the integrators under investigation is shown in Fig. 5.

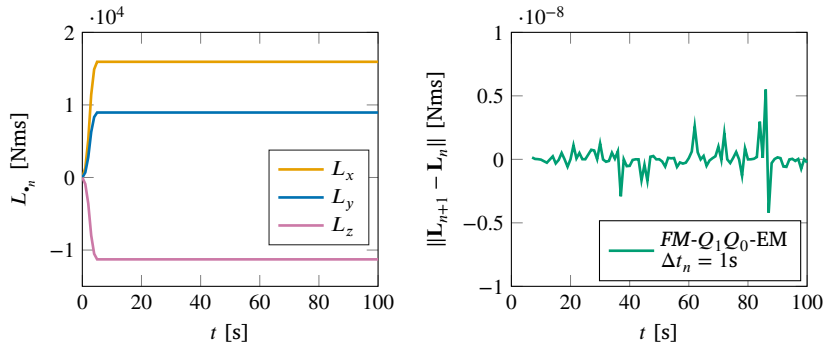

Fig. 5. Illustration of the angular momentum components (left) and norm of the time difference of the angular momentum (right) for the L-shaped body, obtained with *FM*-Q_1Q_0-EM, and time step $\Delta t_n = 1$.

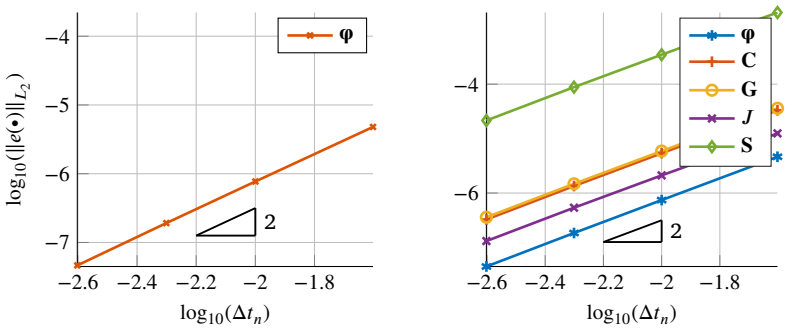

Fig. 6. Numerical accuracy for *RD*-Q_1-EM (left) and *FM*-Q_1Q_0-EM (right).

As evident in the energy diagram (see Fig. 4), the implicit midpoint rule applied to the standard displacement formulation *SD*-Q_1-MP leads to a simulation failure due to an energy blow-up. In contrast, the size-reduced displacement formulation *RD*-Q_1Q_0-EM yields both numerical stability and exact energy conservation (after the loading phase $t > 5\,\mathrm{s}$), as illustrated in Fig. 4.

It should be noted that the other formulations considered, *FM*-Q_1Q_0-EM, *RM*-Q_1Q_0-EM and *SD*-Q_1-EM, also conserve the energy exactly (after the loading phase $t > 5\mathrm{s}$). In addition to that, all considered integrators conserve the angular momentum (after the loading phase $t > 5\mathrm{s}$).

Furthermore, we examine the order of accuracy of the proposed integrators. Analogously to the implicit midpoint rule, second-order convergence is expected. To assess this, we define the relative L_2-norm of the error for a quantity $(\bullet)$ as

$$||e(\bullet)||_{L_2} = \frac{||(\bullet) - (\bullet)_\mathrm{r}||_{L^2}}{||(\bullet)_\mathrm{r}||_{L^2}}\,, \tag{115}$$

with

$$||(\bullet)||_{L_2} = \sqrt{\int_{B_0} ((\bullet)\cdot(\bullet))\,\mathrm{dV}}\,. \tag{116}$$

Here, $(\bullet)_\mathrm{r}$ denotes the reference solution of $(\bullet)$, obtained using the smallest time-step size. For validation, we consider the free-flight motion of the L-shaped block in the time interval $5\mathrm{s} \le t \le 6\mathrm{s}$. As illustrated in Fig. 6 in a double logarithmic scale, the proposed *RD*-Q_1Q_0-EM and *FM*-Q_1Q_0-EM formulations exhibit second-order accuracy.

6.2. Dynamics of a bending and twisting beam

The objective of this second example is to investigate numerical robustness and discrete conservation properties in the case of quasi-incompressible material behavior. We primarily apply the size-reduced mixed formulation (Section 5.2), i.e. *RM*-Q_1Q_0-EM and *RM*-Q_2Q_1-EM, since the underlying mixed finite element formulation has been shown to be well suited for quasi-incompressible finite elasticity (see [25,26]).

The underlying examples originate from [38,39]. For the pure bending beam, see also [17]. The geometry and initial setting with boundary conditions are shown in Fig. 7.

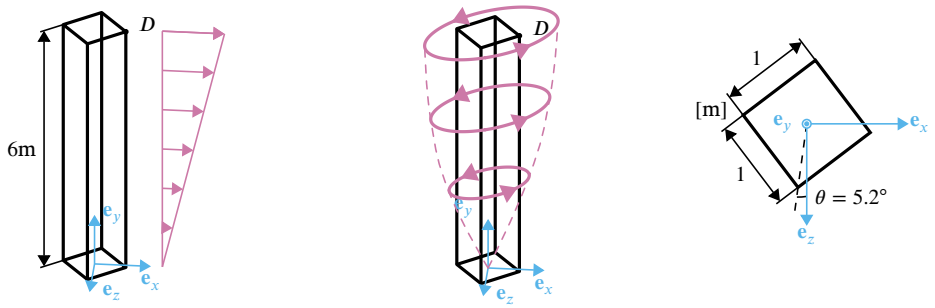

Fig. 7. Geometric setup of the beam in its initial configuration and initial velocities: bending beam (left), twisting beam (center), and top view (right).

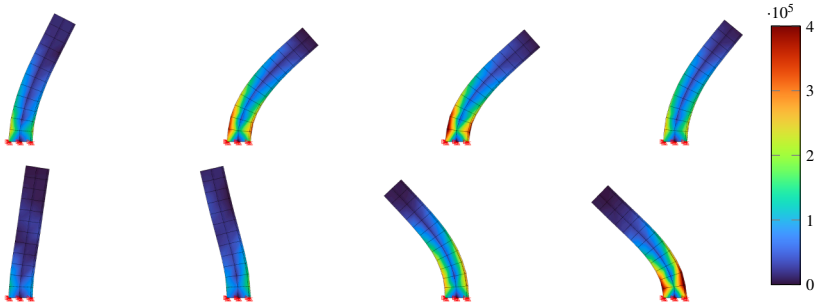

Fig. 8. Snapshots of the bending beam problem for the *RM*-Q_1Q_0-EM formulation with von Mises stress distribution σ_{vM} [Pa] at times $t \in \{0.2, 0.4, 0.6, 0.8, 1.0, 1.2, 1.4, 1.6\}$s.

In particular, the initial velocities for bending and twisting, respectively, illustrated in Fig. 7, are given by

$$\mathbf{v}^{\text{bending}}(\mathbf{x}, t=0) = \begin{bmatrix} 5y/3 \\ 0 \\ 0 \end{bmatrix} \left[\frac{\text{m}}{\text{s}}\right], \quad \mathbf{v}^{\text{twisting}}(\mathbf{x}, t=0) = 100 \sin\left(\frac{\pi y}{12}\right) \begin{bmatrix} z \\ 0 \\ -x \end{bmatrix} \left[\frac{\text{m}}{\text{s}}\right]. \tag{117}$$

Accordingly, due to the asymmetric clamping with respect to the coordinate system and the initial velocity, the bending beam problem is non-symmetric. In contrast to the examples in [39], which employ a Saint-Venant-Kirchhoff constitutive model, and [17,38], which both use a neoHookean model, we consider the modified Mooney-Rivlin model (112) with parameters given in Table 3, both taken from [25]. The parameters lead to nearly incompressible material behavior.

To obtain comparable deformations as in [17,39], we choose a density (see Table 3) that is one-quarter of the value used in [17,39]. A $2 \times 12 \times 2$ finite element mesh is used. The simulations are carried out with the *RM*-Q_1Q_0-EM formulation for the bending beam and the *RM*-Q_2Q_1-EM formulation for the twisting beam. In the case of the bending beam, a total time of $T = 20$s is considered, using a time step size of $\Delta t_n = 0.05$s and a Newton tolerance of $\epsilon = 5e\text{-}5$. For the twisting beam, the parameters are set to $T = 4$ s and $\epsilon = 5e\text{-}6$. The time-step size is chosen as $\Delta t_n = 0.01$ s for the material parameters given in Table 3 and $\Delta t_n = 0.002$ s for the material parameters given in Table 4. Note that a smaller time-step size is required for the more demanding combination of twisting deformation and near-incompressibility ($\nu = 0.499$).

Snapshots of the deformation and von Mises stress distribution are shown in Fig. 8 for the *RM*-Q_1Q_0-EM formulation and Fig. 9 for the *RM*-Q_2Q_1-EM formulation, respectively, while the total energy is depicted in Fig. 10.

Additionally, we compute the *RM*-Q_1Q_0-EM and *RM*-Q_2Q_1-EM formulations for the modified Mooney-Rivlin model with parameters given in Table 4, corresponding to a Poisson's ratio of $\nu = 0.499$. The resulting total energies are shown in Fig. 11. Furthermore, we investigate how accurately quasi-incompressibility is enforced (see Fig. 12) by evaluating the mean error

$$\bar{\mathcal{E}}_J = \frac{1}{V} \int_{\Omega_0} |J - 1| \, \text{dV}, \quad \bar{\mathcal{E}}_{\text{J}_\varphi} = \frac{1}{\text{V}} \int_{\Omega_0} |\text{J}_\varphi - 1| \, \text{dV}, \tag{118}$$

where the total reference volume is given by

$$V = \int_{\Omega_0} \text{dV}. \tag{119}$$

Due to the new rate-type pH formulation, a drift between J and J_φ can be observed. The mixed quantity J therefore tends to fulfill the incompressibility constraint more accurately. This tendency becomes more pronounced in the nearly incompressible case (cf. $\nu = 0.495$ in Fig. 12, left, versus $\nu = 0.499$ in Fig. 12, right). Although the drift between J and J_φ is of interest, only J enters the

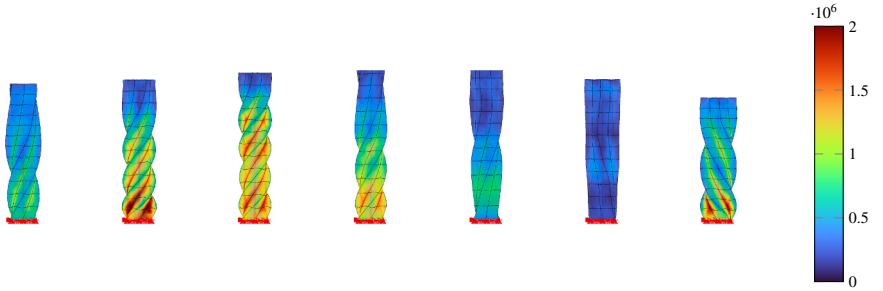

Fig. 9. Snapshots of the twisting beam problem for the $RM\text{-}Q_2Q_1$-EM formulation with von Mises stress distribution σ_{vM} [Pa] at times $t \in \{0.04, 0.08, 0.12, 0.16, 0.20, 0.24, 0.28\}$s.

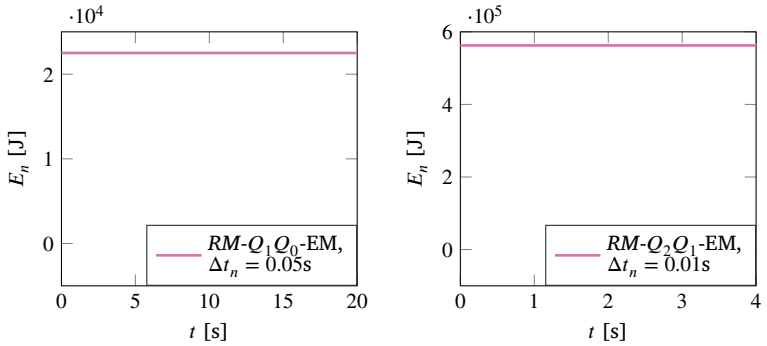

Fig. 10. Total energy of the bending (left) and twisting (right) beam for a quasi-incompressible material with parameters given in Table 3 ($\nu = 0.495$). In both cases, the energy is conserved within the prescribed Newton tolerance.

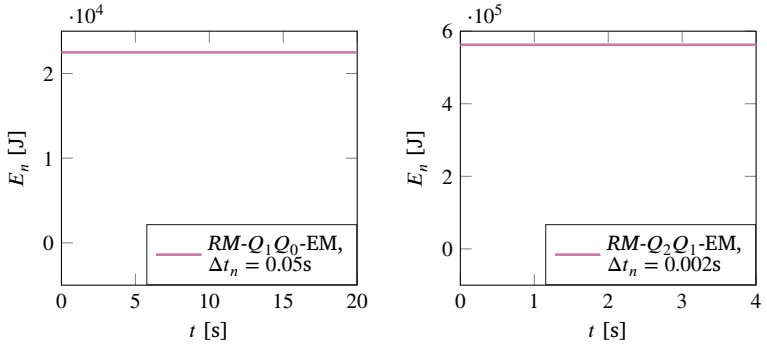

Fig. 11. Total energy of the bending (left) and twisting (right) beam for a quasi-incompressible material with parameters given in Table 4 ($\nu = 0.499$). In both cases, the energy is conserved within the prescribed Newton tolerance.

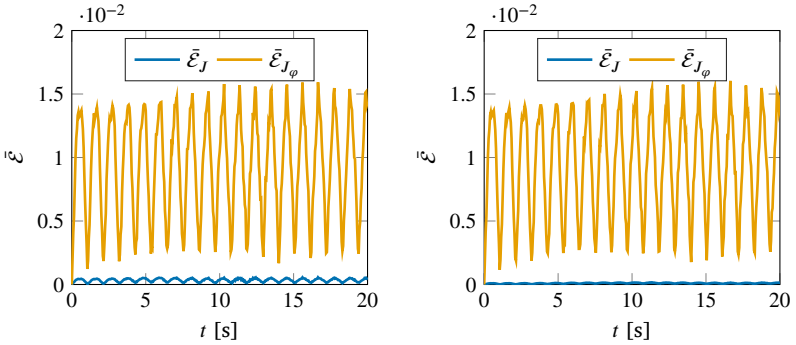

Fig. 12. Verification of quasi-incompressibility for the bending beam using the $RM\text{-}Q_1Q_0$-EM formulation with a time-step size of $\Delta t_n = 0.05$ s. Left: $\nu = 0.495$ with material parameters given in Table 3. Right: $\nu = 0.499$ with material parameters given in Table 4.

strain energy in the formulation, and the incompressibility constraint associated with J is satisfied to a very good degree, as can be observed in Fig. 12.

Despite the relatively coarse time step sizes, the *RM*-Q_1Q_0-EM formulation for the bending beam and the *RM*-Q_2Q_1-EM formulation for the twisting beam remain stable with energy conserved throughout these fully conservative setups.

It should be noted that the fully mixed formulations, i.e. *FM*-Q_1Q_0-EM and *FM*-Q_2Q_1-EM, produce nearly identical results, conserving energy and maintaining stability throughout the entire simulation.

7. Conclusion

We have proposed a new port-Hamiltonian formulation of finite elasticity along with its structure-preserving discretization in space and time. We have shown that the combination of Livens' variational principle with a Hu-Washizu-type extension adapted to polyconvex finite elasticity can be used to (i) derive the continuous pH formulation and (ii) construct a fully mixed weak formulation which provides the foundation for the structure-preserving discretization in space and time.

We have seen that the straightforward spatial discretization of the fully mixed weak formulation leads to semi-discrete equations of motion, which can be put in the form of a discrete pH system. Moreover, the direct temporal discretization of the fully mixed weak formulation provides a framework that accommodates alternative finite element formulations and leads to structure-preserving energy-momentum schemes. In this way, alternative finite elements suitable for handling quasi-incompressible finite elasticity can be chosen and extended to the dynamic regime. This was shown, in particular, for the mixed finite element formulation developed in [25,26].

A unique feature of the underlying pH description is that the strain-displacement relations are written in rate form. In this respect, the present approach bears some similarities with previous developments in [40] and [39]. The main advantage of the present pH-based approach is that it facilitates the design of energy-momentum-consistent methods in a natural way. This has been shown in the context of second-order accurate time-stepping schemes by employing the midpoint rule together with the notion of discrete derivatives applied to the stored energy function.

In essence, the underlying rate form of the strain-displacement relations makes possible the design of energy-momentum-consistent methods for a whole family of mixed finite element formulations that fit into the structure provided by the fully mixed weak form. The corresponding size reduction procedure has been shown for mixed finite elements due to [25,26] (Section 5.2) and pure displacement elements (Section 5.3). This is in contrast to previous related work [24], which requires a specific cascade form of strain-type variables and thus precludes the use of other previously developed mixed finite elements for finite elastostatics, which in general do not comply with the cascade form of strain-type variables.

On the other hand, the versatility of the present pH-based approach comes at the expense of strain-type history variables that need to be retrieved from storage at the element level in each time step. In particular, strain-type history variables emerge in the static condensation procedure of mixed finite elements and for fully reduced displacement elements. In fact, this specific feature distinguishes the pH-based approach from previously designed EM methods. Similar observations have been made in the context of the nonlinear beam model investigated in [11].

Future research can address the extension of the present approach to multiphysics as well as inelastic material models, further exhausting the possibilities of the port-Hamiltonian framework. The present approach also opens promising avenues for the area of control, where energy-based formulations are of central importance.

CRediT authorship contribution statement

Moritz Hille: Writing – review & editing, Writing – original draft, Visualization, Validation, Software, Project administration, Methodology, Formal analysis, Conceptualization; **Peter Betsch:** Writing – review & editing, Writing – original draft, Validation, Supervision, Resources, Project administration, Methodology, Funding acquisition, Formal analysis, Conceptualization; **Marlon Franke:** Writing – review & editing, Writing – original draft, Visualization, Validation, Software, Project administration, Methodology, Investigation, Funding acquisition, Formal analysis, Data curation, Conceptualization.

Data availability

The source code for the finite element computations is implemented in MATLAB, released under the MIT license, and available in https://github.com/kit-ifm/moofeKIT. The version of the code used in this study (v1.0.4) is archived in [41].

Declaration of competing interest

The authors declare that they have no known competing financial interests or personal relationships that could have appeared to influence the work reported in this paper.

Acknowledgements

P. Betsch acknowledges the financial support provided by the Deutsche Forschungsgemeinschaft (DFG, German Research Foundation, project number 388118188). M. Franke acknowledges the financial support provided by the Deutsche Forschungsgemeinschaft (DFG, German Research Foundation, project number 443238377).

Appendix A. Appendix

A.1. Nodal operator matrix

The nodal operator matrix $\mathbb{B}_{\hat{\boldsymbol{\varphi}}}$ is defined such that

$$\operatorname{sym}(\mathbf{F}_{\boldsymbol{\varphi}^{\mathrm{h}}}^{\mathrm{T}} \nabla \mathbf{w}_{\varphi}^{\mathrm{h}}) : \mathbf{A} = \{\mathbf{A}\}_{\mathrm{V}}^{\mathrm{T}} \mathbb{B}_{\hat{\boldsymbol{\varphi}}} \hat{\mathbf{w}}_{\varphi} \tag{A.1}$$

holds for any symmetric second-order tensor $\mathbf{A}$. Since

$$\begin{aligned} \operatorname{sym}(\mathbf{F}_{\boldsymbol{\varphi}^{\mathrm{h}}}^{\mathrm{T}} \nabla \mathbf{w}_{\varphi}^{\mathrm{h}}) : \mathbf{A} &= \mathbf{A} : \left(\mathbf{F}_{\boldsymbol{\varphi}^{\mathrm{h}}}^{\mathrm{T}} \nabla \mathbf{w}_{\varphi}^{\mathrm{h}} \right) \\ &= \operatorname{tr}\left(\mathbf{A}^{\mathrm{T}} \mathbf{F}_{\boldsymbol{\varphi}^{\mathrm{h}}}^{\mathrm{T}} \nabla \mathbf{w}_{\varphi}^{\mathrm{h}} \right) \\ &= \sum_{K=1}^{n_{\mathrm{node}}} \operatorname{tr}\left(\mathbf{A}^{\mathrm{T}} \mathbf{F}_{\boldsymbol{\varphi}^{\mathrm{h}}}^{\mathrm{T}} \hat{\mathbf{w}}_{\varphi}^{K} \otimes \nabla N_{\varphi}^{K} \right) \\ &= \sum_{K=1}^{n_{\mathrm{node}}} \nabla N_{\varphi}^{K} \cdot \left(\mathbf{A}^{\mathrm{T}} \mathbf{F}_{\boldsymbol{\varphi}^{\mathrm{h}}}^{\mathrm{T}} \hat{\mathbf{w}}_{\varphi}^{K} \right) \\ &= \{\mathbf{A}\}_{\mathrm{V}}^{\mathrm{T}} \Big(\sum_{K=1}^{n_{\mathrm{node}}} \mathbb{B}_{\hat{\boldsymbol{\varphi}}}^{K} \hat{\mathbf{w}}_{\varphi}^{K} \Big) \, . \end{aligned} \tag{A.2}$$

Note that $\mathbb{B}_{\hat{\boldsymbol{\varphi}}}^{K}$ is linear in the nodal position vectors, because

$$\mathbf{F}_{\boldsymbol{\varphi}^{\mathrm{h}}} = \nabla \boldsymbol{\varphi}^{\mathrm{h}} = \sum_{K=1}^{n_{\mathrm{node}}} \hat{\boldsymbol{\varphi}}^{K} \otimes \nabla N_{\varphi}^{K} \, . \tag{A.3}$$

Now, it can be inferred from (A.2) that the nodal operator matrix $\mathbb{B}_{\hat{\boldsymbol{\varphi}}}$ is given by

$$\mathbb{B}_{\hat{\boldsymbol{\varphi}}} = \left[\mathbb{B}_{\hat{\boldsymbol{\varphi}}}^{1} \quad \cdots \quad \mathbb{B}_{\hat{\boldsymbol{\varphi}}}^{n_{\mathrm{node}}} \right] , \tag{A.4}$$

where

$$\mathbb{B}_{\hat{\boldsymbol{\varphi}}}^{K} = \begin{bmatrix} F_{11} N_{,x}^{K} & F_{21} N_{,x}^{K} & F_{31} N_{,x}^{K} \\ F_{12} N_{,y}^{K} & F_{22} N_{,y}^{K} & F_{32} N_{,y}^{K} \\ F_{13} N_{,z}^{K} & F_{23} N_{,z}^{K} & F_{33} N_{,z}^{K} \\ F_{11} N_{,y}^{K} + F_{12} N_{,x}^{K} & F_{21} N_{,y}^{K} + F_{22} N_{,x}^{K} & F_{31} N_{,y}^{K} + F_{32} N_{,x}^{K} \\ F_{12} N_{,z}^{K} + F_{13} N_{,y}^{K} & F_{22} N_{,z}^{K} + F_{23} N_{,y}^{K} & F_{32} N_{,z}^{K} + F_{33} N_{,y}^{K} \\ F_{11} N_{,z}^{K} + F_{13} N_{,x}^{K} & F_{21} N_{,z}^{K} + F_{23} N_{,x}^{K} & F_{31} N_{,z}^{K} + F_{33} N_{,x}^{K} \end{bmatrix} . \tag{A.5}$$

A.2. Matrix related to the tensor cross product

The matrix representation of the tensor cross product of second-order tensors is defined such that the relationship

$$(\mathbf{O} \gg \mathbf{P}) : \mathbf{Q} = \{\mathbf{O}\}_{\mathrm{V}}^{\mathrm{T}} \mathcal{D}(\mathbf{Q}) \{\mathbf{P}\}_{\mathrm{V}} \tag{A.6}$$

holds for a symmetric second-order tensor $\mathbf{Q}$, a symmetric strain-like second-order tensor $\mathbf{O}$ and a symmetric stress-like second-order tensor $\mathbf{P}$. Using definition (2) of the tensor cross product, the last equation can be written in index notation as

$$\begin{aligned} (\mathbf{O} \gg \mathbf{P}) : \mathbf{Q} &= \epsilon_{i\alpha\beta} \epsilon_{jab} O_{\alpha a} P_{\beta b} Q_{ij} \\ &= O_{\alpha a} Q_{ij} \epsilon_{i\alpha\beta} \epsilon_{jab} P_{\beta b} \end{aligned} \tag{A.7}$$

Now, comparing the last equation with the right-hand side of (A.6) and taking into account the summation convention, the properties of the permutation symbol along with the Voigt notations in (68), one obtains

$$\mathcal{D}(\mathbf{Q}) = \begin{bmatrix} 0 & Q_{33} & Q_{22} & 0 & -2Q_{23} & 0 \\ Q_{33} & 0 & Q_{11} & 0 & 0 & -2Q_{13} \\ Q_{22} & Q_{11} & 0 & -2Q_{12} & 0 & 0 \\ 0 & 0 & -Q_{12} & -Q_{33} & Q_{13} & Q_{23} \\ -Q_{23} & 0 & 0 & Q_{13} & -Q_{11} & Q_{12} \\ 0 & -Q_{13} & 0 & Q_{23} & Q_{12} & -Q_{22} \end{bmatrix} . \tag{A.8}$$

Note that matrix $\mathcal{D}(\mathbf{Q})$ is not symmetric, since the Voigt notation for $\mathbf{O}$ and $\mathbf{P}$ differs in off-diagonal terms. Additionally, it should be noted that the matrix $\mathcal{D}(\mathbf{Q})$ would be symmetric if Mandel notation was employed in place of classical Voigt notation.

A.3. Update formula for the reduced mixed formulation

We show that for the reduced mixed formulations dealt with in Sections 5.2 and 5.3, the update formula for $\mathbf{C}_{n+1}$ in (53) yields the result $\mathbf{C}_{n+1} = \mathbf{C}_{\varphi^{\mathrm{h}}_{n+1}}$. Thus, from (53), we have

$$\int_{\Omega_0} \mathbf{w}_{\mathbf{\Lambda}_{\mathbf{C}}} : \left[\mathbf{C}_{n+1} - \mathbf{C}_n - 2\Delta t_n \,\mathrm{sym}(\mathbf{F}^{\mathrm{T}}_{\varphi^{\mathrm{h}}_{n+1/2}} \nabla \mathbf{v}^{\mathrm{h}}_{n+1/2})\right] \mathrm{dV} = 0 \,. \tag{A.9}$$

Due to the arbitrariness of $\mathbf{w}_{\mathbf{\Lambda}_{\mathbf{C}}} \in \mathcal{V}_C$, the last equation yields

$$\mathbf{C}_{n+1} - \mathbf{C}_n = \Delta t_n 2\,\mathrm{sym}(\mathbf{F}^{\mathrm{T}}_{\varphi^{\mathrm{h}}_{n+1/2}} \nabla \mathbf{v}^{\mathrm{h}}_{n+1/2}) \,. \tag{A.10}$$

Now,

$$2\,\mathrm{sym}(\mathbf{F}^{\mathrm{T}}_{\varphi^{\mathrm{h}}_{n+1/2}} \nabla \mathbf{v}^{\mathrm{h}}_{n+1/2}) = \mathbf{F}^{\mathrm{T}}_{\varphi^{\mathrm{h}}_{n+1/2}} \nabla \mathbf{v}^{\mathrm{h}}_{n+1/2} + (\nabla \mathbf{v}^{\mathrm{h}}_{n+1/2})^{\mathrm{T}} \mathbf{F}_{\varphi^{\mathrm{h}}_{n+1/2}} \,. \tag{A.11}$$

Taking into account

$$\begin{aligned} \mathbf{F}_{\varphi^{\mathrm{h}}_{n+1/2}} &= \nabla \boldsymbol{\varphi}^{\mathrm{h}}_{n+1/2} = \frac{1}{2}\left(\nabla \boldsymbol{\varphi}^{\mathrm{h}}_n + \nabla \boldsymbol{\varphi}^{\mathrm{h}}_{n+1}\right) \,, \\ \nabla \mathbf{v}^{\mathrm{h}}_{n+1/2} &= \frac{1}{\Delta t_n} \nabla \left(\boldsymbol{\varphi}^{\mathrm{h}}_{n+1} - \boldsymbol{\varphi}^{\mathrm{h}}_n\right) = \frac{1}{\Delta t_n}\left(\nabla \boldsymbol{\varphi}^{\mathrm{h}}_{n+1} - \nabla \boldsymbol{\varphi}^{\mathrm{h}}_n\right) \,, \end{aligned} \tag{A.12}$$

we obtain

$$\begin{aligned} \Delta t_n 2\,\mathrm{sym}(\mathbf{F}^{\mathrm{T}}_{\varphi^{\mathrm{h}}_{n+1/2}} \nabla \mathbf{v}^{\mathrm{h}}_{n+1/2}) &= (\nabla \boldsymbol{\varphi}^{\mathrm{h}}_{n+1})^{\mathrm{T}} \nabla \boldsymbol{\varphi}^{\mathrm{h}}_{n+1} - (\nabla \boldsymbol{\varphi}^{\mathrm{h}}_n)^{\mathrm{T}} \nabla \boldsymbol{\varphi}^{\mathrm{h}}_n \\ &= \mathbf{C}_{\varphi^{\mathrm{h}}_{n+1}} - \mathbf{C}_{\varphi^{\mathrm{h}}_n} \,. \end{aligned} \tag{A.13}$$

Consequently, (A.10) yields

$$\mathbf{C}_{n+1} - \mathbf{C}_n = \mathbf{C}_{\varphi^{\mathrm{h}}_{n+1}} - \mathbf{C}_{\varphi^{\mathrm{h}}_n} \tag{A.14}$$

and thus $\mathbf{C}_{n+1} = \mathbf{C}_{\varphi^{\mathrm{h}}_{n+1}}$ provided that $\mathbf{C}_n = \mathbf{C}_{\varphi^{\mathrm{h}}_n}$.

Supplementary material

Supplementary material associated with this article can be found in the online version at 10.1016/j.cma.2026.118790

References

[1] V. Duindam, A. Macchelli, S. Stramigioli, H. Bruyninckx (Eds.), Modeling and Control of Complex Physical Systems. The Port-Hamiltonian Approach, Springer-Verlag, Berlin, Heidelberg, Berlin, Heidelberg, 2009. https://doi.org/10.1007/978-3-642-03196-0

[2] A.J. van der Schaft, D. Jeltsema, Port-hamiltonian systems theory: an introductory overview, Found. Trend. Syst. Control 1 (2–3) (2014) 173–378. https://doi.org/10.1561/2600000002

[3] B.M. Maschke, A.J. van der Schaft, Port-Controlled hamiltonian systems: modelling origins and systemtheoretic properties, IFAC Proc. Vols. 25 (13) (1992) 359–365. 2nd IFAC Symposium on Nonlinear Control Systems Design 1992, Bordeaux, France, 24–26 June. https://doi.org/10.1016/S1474-6670(17)52308-3

[4] A.J. van der Schaft, B.M. Maschke, Hamiltonian formulation of distributed-parameter systems with boundary energy flow, J. Geom. Phys. 42 (1–2) (2002) 166–194. https://doi.org/10.1016/S0393-0440(01)00083-3

[5] R. Rashad, F. Califano, A.J. van der Schaft, S. Stramigioli, Twenty years of distributed port-hamiltonian systems: a literature review, IMA J. Math. Control Inf. 37 (1) (2020) 1400–1422. https://doi.org/10.1093/imamci/dnaa018

[6] P. Kotyczka, B. Maschke, L. Lefèvre, Weak form of stokes–dirac structures and geometric discretization of port-hamiltonian systems, J. Comput. Phys. 361 (2018) 442–476. https://doi.org/10.1016/j.jcp.2018.02.006

[7] P.L. Kinon, T. Thoma, P. Betsch, P. Kotyczka, Generalized maxwell viscoelasticity for geometrically exact strings: nonlinear port-hamiltonian formulation and structure-preserving discretization, IFAC-PapersOnLine 58 (6) (2024) 101–106. https://doi.org/10.1016/j.ifacol.2024.08.264

[8] F.L. Cardoso-Ribeiro, D. Matignon, V. Pommier-Budinger, Piezoelectric beam with distributed control ports: a power-preserving discretization using weak formulations, IFAC-PapersOnLine 49 (8) (2016) 290–297. https://doi.org/10.1016/j.ifacol.2016.07.456

[9] A. Brugnoli, R. Rashad, F. Califano, S. Stramigioli, D. Matignon, Mixed finite elements for port-hamiltonian models of von kármán beams, IFAC-PapersOnLine 54 (19) (2021) 186–191. https://doi.org/10.1016/j.ifacol.2021.11.076

[10] C. Ponce, H. Ramirez, Y. Le Gorrec, Y. Wu, Constrained port-hamiltonian modeling and structure-preserving discretization of the rayleigh beam, IFAC-PapersOnLine 59 (8) (2025) 108–113. https://doi.org/10.1016/j.ifacol.2025.08.075

[11] P.L. Kinon, P. Betsch, S.R. Eugster, Energy-momentum-consistent simulation of planar geometrically exact beams in a port-hamiltonian framework, Multibody Syst. Dyn. (2025). https://doi.org/10.1007/s11044-025-10087-9

[12] A. Brugnoli, D. Alazard, V. Pommier-Budinger, D. Matignon, Structure-preserving discretization of port-hamiltonian plate models, IFAC-PapersOnLine 54 (39) (2021) 359–364. https://doi.org/10.1016/j.ifacol.2021.06.094

[13] F.L. Cardoso-Ribeiro, D. Matignon, L. Lefèvre, A structure-preserving partitioned finite element method for the 2d wave equation, IFAC-PapersOnLine 51 (3) (2018) 119–124. https://doi.org/10.1016/J.IFACOL.2018.06.033

[14] R. Altmann, V. Mehrmann, B. Unger, Port-hamiltonian formulations of poroelastic network models, Math. Comput. Model. Dyn. Syst. 27 (1) (2021) 429–452. https://doi.org/10.1080/13873954.2021.1975137

[15] A. Brugnoli, D. Alazard, V. Pommier-Budinger, D. Matignon, A port-hamiltonian formulation of linear thermoelasticity and its mixed finite element discretization, J. Therm. Stresses 44 (6) (2021) 643-661. https://doi.org/10.1080/01495739.2021.1917322

[16] T. Thoma, P. Kotyczka, H. Egger, On the velocity-stress formulation for geometrically nonlinear elastodynamics and its structure-preserving discretization, Math. Comput. Model. Dyn. Syst. 30 (1) (2024) 701–720. https://doi.org/10.1080/13873954.2024.2397486

[17] A. Brugnoli, D. Matignon, J. Morlier, A linearly-implicit energy-momentum preserving scheme for geometrically nonlinear mechanics based on non-canonical hamiltonian formulations, Nonlinear Dyn. (2025). https://doi.org/10.1007/s11071-025-11601-6
[18] C. Ponce, Y. Wu, Y. Le Gorrec, H. Ramirez, A port-hamiltonian framework for the modeling and FEM discretization of hyperelastic systems, Appl. Math. Model. (2025) 116403. https://doi.org/10.1016/j.apm.2025.116403
[19] J. Simo, N. Tarnow, The discrete energy-momentum method. conserving algorithms for nonlinear elastodynamics, Zeitschrift für angewandte Mathematik und Physik ZAMP 43 (1992) 757–792. https://doi.org/10.1007/BF00913408
[20] O. Gonzalez, Exact energy and momentum conserving algorithms for general models in nonlinear elasticity, Comput. Methods Appl. Mech. Engrg. 190 (2000) 1763–1783. https://doi.org/10.1016/S0045-7825(00)00189-4
[21] I. Romero, An analysis of the stress formula for energy-momentum methods in nonlinear elastodynamics, Comput. Mech. 50 (5) (2012) 603–610. https://doi.org/10.1007/s00466-012-0693-y
[22] P. Betsch, P. Steinmann, Conservation properties of a time FE method. part II: time-Stepping schemes for nonlinear elastodynamics, Int. J. Numer. Meth. Engng. 50 (2001) 1931–1955. https://doi.org/10.1002/nme.103
[23] M. Groß, P. Betsch, P. Steinmann, Conservation properties of a time FE method. part IV: higher order energy and momentum conserving schemes, Int. J. Numer. Meth. Engng. 63 (2005) 1849–1897. https://doi.org/10.1002/nme.1339
[24] P. Betsch, A. Janz, C. Hesch, A mixed variational framework for the design of energy-momentum schemes inspired by the structure of polyconvex stored energy functions, Comput. Methods Appl. Mech. Eng. 335 (2018) 660–696. https://doi.org/10.1016/j.cma.2018.01.013
[25] J. Schröder, P. Wriggers, D. Balzani, A new mixed finite element based on different approximations of the minors of deformation tensors, Comput. Methods Appl. Mech. Eng. 200 (2011) 3583–3600. https://doi.org/10.1016/j.cma.2011.08.009
[26] A. Kraus, P. Wriggers, N. Viebahn, J. Schröder, Low-order locking-free mixed finite element formulation with approximation of the minors of the deformation gradient, Int. J. Numer. Meth. Engng. 120 (8) (2019) 1011–1026. https://doi.org/10.1002/nme.6168
[27] R. de Boer, Vektor- und Tensorrechnung für Ingenieure, Springer-Verlag Berlin Heidelberg, 1982 https://doi.org/10.1002/zamm.19840640614.
[28] J. Bonet, A.J. Gil, R. Ortigosa, On a tensor cross product based formulation of large strain solid mechanics, Int. J. Solids Struct. 84 (2016) 49–63. https://doi.org/10.1016/j.ijsolstr.2015.12.030
[29] P.L. Kinon, P. Betsch, S. Schneider, Structure-preserving integrators based on a new variational principle for constrained mechanical systems, Nonlinear Dyn. 111 (2023) 14231-14261. https://doi.org/10.1007/s11071-023-08522-7
[30] K. Washizu, Variational Methods in Elasticity and Plasticity, Pergamon Press, 2nd edition, 1975 https://doi.org/10.1002/zamm.19690490535.
[31] V. Mehrmann, R. Morandin, Structure-preserving discretization for port-hamiltonian descriptor systems, in: Proceedings of the 58Th IEEE Conference on Decision and Control, Nice, France, 2019, pp. 6863–6868. https://doi.org/10.1109/CDC40024.2019.9030180
[32] V. Mehrmann, B. Unger, Control of port-hamiltonian differential-algebraic systems and applications, Acta Numerica 32 (2023) 395–515. https://doi.org/10.1017/S0962492922000083
[33] O. Gonzalez, Time integration and discrete hamiltonian systems, J. Nonlinear Sci. 6 (5) (1996) 449–467. https://doi.org/10.1007/BF02440162
[34] D. Greenspan, Conservative numerical methods for $\ddot{x} = f(x)$, J. Comput. Phys. 56 (1) (1984) 28–41. https://doi.org/10.1016/0021-9991(84)90081-0
[35] P. Wriggers, Nonlinear Finite Element Methods, Springer, Berlin; Heidelberg, Berlin; Heidelberg, 2008. https://doi.org/10.1007/978-3-540-71001-1
[36] M. Franke, D.K. Klein, O. Weeger, P. Betsch, Advanced discretization techniques for hyperelastic physics-augmented neural networks, Comput. Methods Appl. Mech. Eng. 416 (2023). https://doi.org/10.1016/j.cma.2023.116333
[37] M. Franke, A. Janz, M. Schiebl, P. Betsch, An energy-momentum consistent integration scheme using a polyconvexity-based framework for non-linear thermo-elastodynamics, Int. J. Numer. Methods Eng. 115 (5) (2018) 549–577. https://doi.org/10.1002/nme.5816
[38] A.J. Gil, C.H. Lee, J. Bonet, M. Aguirre, A stabilised petrov–Galerkin formulation for linear tetrahedral elements in compressible, nearly incompressible and truly incompressible fast dynamics, Comput. Methods Appl. Mech. Eng. 276 (2014) 659–690. https://doi.org/10.1016/j.cma.2014.04.006
[39] G. Scovazzi, B. Carnes, X. Zeng, S. Rossi, A simple, stable, and accurate linear tetrahedral finite element for transient, nearly, and fully incompressible solid dynamics: a dynamic variational multiscale approach, Int. J. Numer. Methods Eng. 106 (2016) 799–839. https://doi.org/10.1002/nme.5138
[40] J. Bonet, A.J. Gil, C.H. Lee, M. Aguirre, R. Ortigosa, A first order hyperbolic framework for large strain computational solid dynamics. part i: total lagrangian isothermal elasticity, Comput. Methods Appl. Mech. Engrg. 283 (2015) 689–732. https://doi.org/10.1016/j.cma.2014.09.024
[41] M. Franke, F. Zähringer, M. Hille, P. Kinon, P. Reiff, MoofeKIT: MATLAB object-oriented finite element KIT, v1.0.4, 2025, https://doi.org/10.5281/zenodo.17235465